SIAM J. SCI. COMPUT.
Vol. 41, No. 6, pp. A3673–A3702

A NOVEL INTEGRAL EQUATION FOR SCATTERING BY LOCALLY ROUGH SURFACES AND APPLICATION TO THE INVERSE PROBLEM: THE NEUMANN CASE*

FENGLONG QU†, BO ZHANG‡, AND HAIWEN ZHANG§

Abstract. This paper is concerned with direct and inverse scattering by a locally perturbed infinite plane (called a locally rough surface in this paper) on which a Neumann boundary condition is imposed. A novel integral equation formulation is proposed for the direct scattering problem which is defined on a bounded curve (consisting of a bounded part of the infinite plane containing the local perturbation and the lower part of a circle) with two corners and some closed smooth artificial curve. It is a nontrivial extension of our previous work on direct and inverse scattering by a locally rough surface from the Dirichlet boundary condition to the Neumann boundary condition [*SIAM J. Appl. Math.*, 73 (2013), pp. 1811–1829]. For the Dirichlet boundary condition, the integral equation obtained is uniquely solvable in the space of bounded continuous functions on the bounded curve, and it can be solved efficiently by using the Nyström method with a graded mesh. However, the Neumann condition case leads to an integral equation which is solvable in the space of squarely integrable functions on the bounded curve rather than in the space of bounded continuous functions, making the integral equation very difficult to solve numerically with the classic and efficient Nyström method. In this paper, we make use of the recursively compressed inverse preconditioning method developed by Helsing to solve the integral equation which is efficient and capable of dealing with large wave numbers. For the inverse problem, it is proved that the locally rough surface is uniquely determined from a knowledge of the far-field pattern corresponding to incident plane waves. Moreover, based on the novel integral equation formulation, a Newton iteration method is developed to reconstruct the locally rough surface from a knowledge of multiple frequency far-field data. Numerical examples are also provided to illustrate that the reconstruction algorithm is stable and accurate even for the case of multiple-scale profiles.

Key words. integral equation, locally rough surface, Neumann boundary condition, far-field pattern, RCIP method, Newton iteration method

AMS subject classifications. 35R30, 35Q60, 65R20, 65N21, 78A46

DOI. 10.1137/19M1240745

1. Introduction.

This paper is concerned with the problem of scattering of plane acoustic or electromagnetic waves by a locally perturbed, perfectly reflecting, infinite plane (which is called a locally rough surface). Such problems arise in many applications such as geophysics, radar, medical imaging, remote sensing, and nondestructive testing (see, e.g., [2, 6, 10, 14, 28]).

In this paper we are restricted to the two-dimensional case by assuming that the local perturbation is invariant in the x_3 direction. Precisely, let $\Gamma := \{(x_1, x_2) \mid x_2 =$

*Submitted to the journal's Methods and Algorithms for Scientific Computing section January 25, 2019; accepted for publication (in revised form) September 27, 2019; published electronically November 19, 2019.

https://doi.org/10.1137/19M1240745

Funding: This work was supported by the NNSF of China under grants 11871416, 11871466, and 91630309 and by the Shandong Provincial Natural Science Foundation through projects ZR2019MA027 and ZR2017MA044.

†School of Mathematics and Informational Science, Yantai University, Yantai, Shandong, 264005, China (fenglongqu@amss.ac.cn).

‡NCMIS, LSEC, and Academy of Mathematics and Systems Science, Chinese Academy of Sciences, Beijing, 100190, China, and School of Mathematical Sciences, University of Chinese Academy of Sciences, Beijing 100049, China (b.zhang@amt.ac.cn).

§Corresponding author. NCMIS and Academy of Mathematics and Systems Science, Chinese Academy of Sciences, Beijing 100190, China, and Institute for Numerical and Applied Mathematics, University of Göttingen, Lotzestr. 16-18, 37083 Göttingen, Germany (zhanghaiwen@amss.ac.cn).

$h(x_1), x_1 \in \mathbb{R}\}$ be the locally rough surface with a smooth function $h \in C^2(\mathbb{R})$ having a compact support in $\mathbb{R}$. Denote by $D_+ = \{(x_1, x_2) \mid x_2 > h(x_1), x_1 \in \mathbb{R}\}$ the unbounded domain above the surface Γ which is filled with a homogeneous medium. Denote by $k = \omega/c > 0$ the wave number of the wave field in D_+, where ω and c are the wave frequency and speed, respectively. We assume throughout the paper that the incident field u^i is the plane wave

$$u^i(x; d) = \exp(ikd \cdot x),$$

where $d = (\sin\theta, -\cos\theta) \in \mathbb{S}^1_-$ is the incident direction, θ is the angle of incidence with $-\pi/2 < \theta < \pi/2$, and $\mathbb{S}^1_- := \{x = (x_1, x_2) \mid |x| = 1, x_2 < 0\}$ is the lower part of the unit circle $\mathbb{S}^1 := \{x \in \mathbb{R}^2 \mid |x| = 1\}$. Notice that the incident wave is time-harmonic ($e^{-i\omega t}$ time dependence), so that the total field u satisfies the Helmholtz equation

$$\Delta u + k^2 u = 0 \quad \text{in } D_+. \tag{1.1}$$

Here, the total field $u = u^i + u^r + u^s$ satisfies the Neumann boundary condition on the surface Γ:

$$\frac{\partial u}{\partial \nu} = \frac{\partial u^i}{\partial \nu} + \frac{\partial u^r}{\partial \nu} + \frac{\partial u^s}{\partial \nu} = 0 \qquad \text{on } \Gamma, \tag{1.2}$$

where ν is the unit normal vector on Γ directed into D_+, u^r is the reflected wave of u^i by the infinite plane $x_2 = 0$,

$$u^r(x; d) = \exp(ik[x_1 \sin\theta + x_2 \cos\theta]),$$

and u^s is the unknown scattered wave to be determined which is required to satisfy the Sommerfeld radiation condition

$$\lim_{r\to\infty} r^{\frac{1}{2}} \left(\frac{\partial u^s}{\partial r} - iku^s\right) = 0, \quad r = |x|, \quad x \in D_+. \tag{1.3}$$

This problem models electromagnetic scattering by a locally perturbed, perfectly reflected, infinite plane in the transverse-magnetic polarization case; it also models acoustic scattering by a one-dimensional sound-hard, locally rough surface (see Figure 2.1 for the geometric configuration of the scattering problem). Further, it can be shown that u^s has the following asymptotic behavior at infinity (see Remark 2.8):

$$u^s(x; d) = \frac{e^{ik|x|}}{\sqrt{|x|}} \left(u^\infty(\hat{x}; d) + O\left(\frac{1}{|x|}\right)\right), \qquad |x| \to \infty,$$

uniformly for all observation directions $\hat{x}=x/|x| \in \mathbb{S}^1_+$ with $\mathbb{S}^1_+ := \{x = (x_1, x_2) \mid |x| = 1, x_2 > 0\}$ the upper part of the unit circle $\mathbb{S}^1$. Here, $u^\infty(\hat{x}; d)$ is called the far-field pattern of the scattered field u^s, depending on the incident direction $d \in \mathbb{S}^1_-$ and the observation direction $\hat{x} \in \mathbb{S}^1_+$.

Direct scattering problems by locally rough surfaces have been studied both numerically and mathematically. For the Dirichlet case, the well-posedness of the scattering problem was first proved in [46] by the integral equation method. In [6], the scattering problem is studied by a variational method, based on a Dirichlet-to-Neumann map, and then solved numerically with using the boundary element method. In [50], a novel integral equation defined on a bounded curve is proposed for the Dirichlet scattering problem, leading to a fast numerical algorithm for the scattering problem, even for large wave numbers. However, for the Neumann case, few results

are available. For the special case when the local perturbation is below the infinite plane (which is called the cavity problem), the well-posedness was established in [1] via the variational method for the direct scattering problem with both Neumann and Dirichlet boundary conditions. A symmetric coupling method of finite element and boundary integral equations was developed in [2], which can be applied to arbitrarily shaped and filled cavities with Neumann or Dirichlet boundary conditions. In the recent [3], the scattering problem by using a locally perturbed interface is studied by using a variational method coupled with a boundary integral equation method and numerically solved, based on the finite element method in a truncated bounded domain coupled with the boundary element method. In [31], based on the perfectly matched layer technique, a boundary integral equation method is developed to numerically solve the locally rough surface scattering problem for a layered medium. Note that the method in [31] may also be applied to the cases of other boundary conditions. Moreover, studies on some related scattering problems have also been conducted; see [40] for cavity scattering problems of Maxwell's equations, [13, 26, 27] for problems with impedance or Neumann boundary conditions, and [14, 15, 16, 17, 18, 19, 20, 48] for the nonlocal perturbation case which is called the rough surface scattering problem.

The inverse scattering problem of reconstructing the rough surfaces has also attracted many researchers' attention. For example, many numerical algorithms have been developed for inverse scattering by locally rough surfaces with Dirichlet boundary conditions (see, e.g., [6, 22, 23, 30, 39, 49, 50] and the references quoted). A marching method based on the parabolic integral equation was proposed in [22] for the reconstruction of a locally rough surface with Dirichlet or Neumann boundary conditions from phaseless measurements of the single frequency scattering field at grazing angles, while a Kirsch–Kress decomposition method was given in [42] to recover a locally rough interface on which transmission boundary conditions are satisfied. For numerical recovery of non-locally rough surfaces, we refer to [4, 5, 7, 10, 11, 21, 22, 28, 29, 41, 43, 45]. For inverse cavity scattering, the reader is referred to [2, 32, 40].

In this paper, we extend our previous work in [50] on direct and inverse scattering by a locally rough surface from the Dirichlet condition to the Neumann condition. Precisely, we propose a novel integral equation formulation for the direct scattering problem (1.1)–(1.3), which is defined on a bounded curve (consisting of a bounded part of the infinite plane containing the local perturbation and the lower part of a circle) with two corners and some closed smooth artificial curve. This extension is nontrivial because, for the Dirichlet condition case considered in [50], the integral equation obtained in [50] is uniquely solvable in the space of bounded continuous functions on the bounded curve, and it can be solved efficiently by using the Nyström method with a graded mesh. However, the Neumann boundary condition leads to an integral equation which is not solvable in the space of bounded continuous functions on the bounded curve (see, e.g., [8, 9]). In this paper, the integral equation formulation obtained is proved to be uniquely solvable in the space of squarely integrable functions on the bounded curve. This then leads to the difficulty in solving the integral equation numerically with the classic and efficient Nyström method with a graded mesh which was used previously in [50]. Instead, we make use of the recursively compressed inverse preconditioning (RCIP) method developed by Helsing to solve the integral equation (see [34, 35, 36, 37]) which is fast, accurate, and capable of dealing with large wave numbers. In addition, a further difficulty in our analysis arises in the study of the property of the derived integral equation formulation in the neighborhood of the two

corners of the bounded curve. To overcome this difficulty, we will use the operator boundedness from [12] in combination with some detailed energy estimates.

For the associated inverse scattering problem, based on the mixed reciprocity relation established in this paper, we will prove that the locally rough surface is uniquely determined from a knowledge of the far-field pattern associate with incident plane waves. Further, we develop a Newton iteration method to reconstruct the locally rough surface from a knowledge of multiple frequency far-field data. It should be mentioned that the proposed novel integral equation plays an essential role in solving the direct scattering problem in each iteration.

This paper is organized as follows. In section 2, we first derive a novel integral equation formulation for the scattering problem (1.1)–(1.3) and then prove its unique solvability. In section 3, a fast numerical algorithm, based on the RCIP method, is proposed for solving the novel integral equation, and a numerical example is carried out to illustrate the performance of the algorithm. Section 4 is devoted to the proof of uniqueness in the inverse scattering problem. In section 5, a Newton iteration algorithm with multifrequency far-field data is developed to numerically solve the inverse problem, based on the proposed novel integral equation. Numerical experiments will also be provided to demonstrate that the reconstruction algorithm is stable and accurate even for the case of multiple-scale profiles. Finally, we will give some concluding remarks in section 6.

2. Solvability of the direct problem via the integral equation method. Let $f = -\partial u^i/\partial\nu - \partial u^r/\partial\nu$ on Γ. It is easy to see that f has a compact support on Γ. Then the scattering problem (1.1)–(1.3) can be reformulated as the Neumann problem (NP): Find $u^s \in H^1_{loc}(D_+)$ which satisfies the Helmholtz equation (1.1) in D_+, the Sommerfeld radiation condition (1.3), and the Neumann boundary condition:

$$\frac{\partial u^s}{\partial \nu} = f \quad \text{on} \quad \Gamma. \tag{2.1}$$

We will propose a novel boundary integral equation formulation for the Neumann problem (NP) which is defined on bounded curves and consequently can be solved with cheap computational cost. The boundary integral equation formulation will then be used to establish the well-posedness of the Neumann problem (NP). We first introduce some notation. Define $a := \inf_{x_1\in\mathbb{R}}\{x_1 \mid h(x_1) \neq 0\}, b := \sup_{x_1\in\mathbb{R}}\{x_1 \mid h(x_1) \neq 0\}$, and $\Gamma_p := \{(x_1, x_2) \mid x_1 \in [a, b], x_2 = h(x_1)\}$. Let $B_R := \{x = (x_1, x_2) \in \mathbb{R}^2 \mid |x| < R\}$ be a disk with $R > 0$ large enough so that the local perturbation $\Gamma_p \subset B_R$. Then $\Gamma_R := \Gamma \cap B_R$ represents the part of Γ containing the local perturbation Γ_p of the infinite plane. Let $x_A := (-R, 0), x_B := (R, 0)$ denote the endpoints of Γ_R. For $x = (x_1, x_2) \in \mathbb{R}^2$, let $x^{re} := (x_1, -x_2)$ be the reflection of x about the x_1-axis. Write $\mathbb{R}^2_\pm := \{(x_1, x_2) \in \mathbb{R}^2 \mid x_2 \gtrless 0\}$, $D_R^\pm := B_R \cap D_\pm$, and $\partial B_R^\pm := \partial B_R \cap D_\pm$, where $D_- := \{(x_1, x_2) \mid x_2 < h(x_1), x_1 \in \mathbb{R}\}$. Further, let $\widetilde{D}$ be an auxiliary domain in the interior of D_R^- with a smooth boundary $\widetilde{\Gamma}$. See Figure 2.1 for the geometry of the scattering problem and some notation introduced.

We now have the following uniqueness result for the Neumann problem (NP). For the case when the local perturbation is a cavity the uniqueness result was proved with a variational method in conjunction with a transparent boundary condition (see, e.g., [1, 47]). The proof also works for the general local perturbation case though the following Theorem 2.1 was not given explicitly for this general case in [1, 47]. Here we give a different proof, based on the reflection principle proposed in [50] for dealing with general local perturbations. Detailed discussions on uniqueness of the Neumann

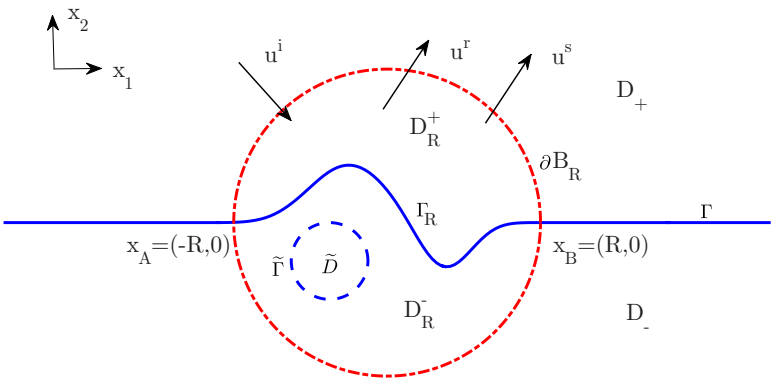

FIG. 2.1. *The scattering problem from a locally rough surface.*

problem can be found in [3, pp. 2675–2677]. Further, uniqueness of the impedance problem was established in [3, subsection 2.2].

THEOREM 2.1. *The Neumann problem* (NP) *has at most one solution* $u^s \in H^1_{loc}(D_+)$.

Proof. Let u^s be the solution of the Neumann problem (NP) with the boundary data $f = 0$. We extend $u^s(x)$ into $\mathbb{R}^2_-\backslash\overline{B}_R$ by reflection, which we still denote by $u^s(x)$, such that $u^s(x) = u^s(x^{re})$ for $x \in \mathbb{R}^2_-\backslash\overline{B}_R$. Then, by the Neumann boundary condition $\partial u^s/\partial\nu = 0$ on $\Gamma\setminus\overline{B}_R$ and the reflection principle we know that u^s satisfies the Helmholtz equation (1.1) in $\mathbb{R}^2\backslash\overline{B}_R$ and the Sommerfeld radiation condition (1.3) uniformly for all directions $\hat{x} = x/|x|$ with $x \in \mathbb{R}^2\backslash\overline{B}_R$.

Now, let $R_0 > R$. By the radiation condition (1.3) it follows that

$$\int_{\partial B^+_{R_0}} \left\{ \left| \frac{\partial u^s}{\partial \nu} \right|^2 + k^2|u^s|^2 + 2k\mathrm{Im}\left(u^s \frac{\partial \overline{u}^s}{\partial \nu} \right) \right\} ds = \int_{\partial B^+_{R_0}} \left| \frac{\partial u^s}{\partial \nu} - iku^s \right|^2 ds \to 0 \tag{2.2}$$

as $R_0 \to +\infty$. On the other hand, using Green's theorem and the Neumann boundary condition on Γ yields

$$\int_{\partial B^+_{R_0}} u^s \frac{\partial \overline{u}^s}{\partial \nu} ds = \int_{B_{R_0}\cap D_+} \left(|\nabla u^s|^2 - k^2|u^s|^2 \right) dx. \tag{2.3}$$

Taking the imaginary part of (2.3), we conclude from (2.2) that

$$\lim_{R_0\to+\infty} \int_{\partial B_{R_0}} \left(\left| \frac{\partial u^s}{\partial \nu} \right|^2 + k^2|u^s|^2 \right) ds = 2 \lim_{R_0\to+\infty} \int_{\partial B^+_{R_0}} \left(\left| \frac{\partial u^s}{\partial \nu} \right|^2 + k^2|u^s|^2 \right) ds = 0.$$

Thus, by Lemma 2.12 in [24] we have $u^s = 0$ in $\mathbb{R}^2\backslash\overline{B}_R$, and so, $u^s = 0$ in $\mathbb{R}^2_+\backslash\overline{B}_R$. This, together with the unique continuation principle [24, Theorem 8.6], implies that $u^s = 0$ in D_+. The proof is thus complete. ∎

In what follows we are going to present two integral equation formulations (2.14) and (2.35) for the Neumann problem (NP). We shall prove that for any wave number k the integral equation (2.14) is well-posed (cf. Theorem 2.4 and Remark 2.5), whereas

the well-posedness of the integral equation (2.35) can be obtained only if k^2 is not a Dirichlet eigenvalue of $-\Delta$ in D_R^- (cf. the arguments below (2.35)). However, the integral equation (2.14) is more expensive computationally than the simpler one (2.35) and thus will be applied to generate synthetic far-field data for the inverse problem, while (2.35) is used to solve the forward scattering problem arising in the iteration algorithm for the inverse problem (see Remark 5.3 for details). To this end, we introduce the layer potentials on the curves Γ_R, ∂B_R^- and $\widetilde{\Gamma}$. For the curve $I_p \in \{\Gamma_R, \partial B_R^-, \widetilde{\Gamma}\}$, define the single-layer potential $\mathcal{S}_{k,I_p}$ by

$$(\mathcal{S}_{k,I_p}\varphi_{I_p})(x) := \int_{I_p} G_k(x,y)\varphi_{I_p}(y)ds(y), \quad x \in \mathbb{R}^2\backslash I_p, \tag{2.4}$$

where $G_k(x,y) := (i/4)H_0^{(1)}(k|x-y|), x, y \in \mathbb{R}^2, x \neq y$, is the fundamental solution of the Helmholtz equation $\Delta w + k^2 w = 0$ in $\mathbb{R}^2$. If the wave number $k = 0$, $G_0(x,y) = -(2\pi)^{-1}\ln|x-y|$ is the fundamental solution of the Laplace equation in $\mathbb{R}^2$. By the asymptotic behavior of the fundamental solution G_k (see, e.g., [24]), the far-field pattern $S_{k,I_p}^{\infty}\varphi_{I_p}$ of the single-layer potential $\mathcal{S}_{k,I_p}\varphi_{I_p}$ can be defined as

$$\left(S_{k,I_p}^{\infty}\varphi_{I_p}\right)(\hat{x}) := \frac{e^{i\pi/4}}{\sqrt{8\pi k}} \int_{I_p} e^{-ik\hat{x}\cdot y}\varphi_{I_p}(y)ds(y), \quad \hat{x} \in \mathbb{S}^1. \tag{2.5}$$

For $I_q \in \{\Gamma_R, \partial B_R^-, \widetilde{\Gamma}\}$, define the boundary integral operators $S_{k,I_p\to I_q}, K'_{k,I_p\to I_q}$:

$$\left(S_{k,I_p\to I_q}\varphi_{I_p}\right)(x) := \int_{I_p} G_k(x,y)\varphi_{I_p}(y)ds(y), \quad x \in I_q, \tag{2.6}$$

$$\left(K'_{k,I_p\to I_q}\varphi_{I_p}\right)(x) := \int_{I_p} \frac{\partial G_k(x,y)}{\partial \nu(x)}\varphi_{I_p}(y)ds(y), \quad x \in I_q, \tag{2.7}$$

where ν is the unit outward normal on ∂D_R^- and $\widetilde{\Gamma}$. Further, define the boundary operator $K'^{,re}_{k,I_p\to\partial B_R^-}$:

$$\left(K'^{,re}_{k,I_p\to\partial B_R^-}\varphi_{I_p}\right)(x) := \int_{I_p} \frac{\partial G_k(x^{re},y)}{\partial \nu(x^{re})}\varphi_{I_p}(y)ds(y), \quad x \in \partial B_R^-,$$

where ν is the unit outward normal on ∂B_R^+ directing into $\mathbb{R}^2\backslash\overline{B}_R$. Some properties of the boundary integral operators $S_{k,I_p\to I_q}$, $K'_{k,I_p\to I_q}$, and $K'^{,re}_{k,I_p\to\partial B_R^-}$ for $I_p, I_q \in \{\Gamma_R, \partial B_R^-, \widetilde{\Gamma}\}$ are presented in Remark 2.2 below. For a comprehensive discussion of mapping properties of the layer potentials, we refer to [24, 44] and the references therein.

Remark 2.2. (i) Let $I_p \in \{\Gamma_R, \partial B_R^-\}$ and $\varphi_{I_p} \in L^2(I_p)$. Since any function in $L^2(I_p)$ can be extended by zero to a function in $L^2(\partial D_R^-)$, it follows from the mapping properties of the single-layer potential over a closed piecewise-smooth boundary (see [44, Chapter 6]) that $\mathcal{S}_{k,I_p}\varphi_{I_p} \in H_{loc}^{3/2}(\mathbb{R}^2)$ satisfies the Helmholtz equation (1.1) in $\mathbb{R}^2\backslash\overline{I_p}$ and the jump relations on the curve I_p:

$$(\mathcal{S}_{k,I_p}\varphi_{I_p})_{\pm}|_{I_p} = S_{k,I_p\to I_p}\varphi_{I_p}, \tag{2.8}$$

$$\left(\frac{\partial}{\partial\nu}\mathcal{S}_{k,I_p}\varphi_{I_p}\right)_{\pm}\Big|_{I_p} = \mp\frac{1}{2}\varphi_{I_p} + K'_{k,I_p\to I_p}\varphi_{I_p}, \tag{2.9}$$

where

$$(\mathcal{S}_{k,I_p}\varphi_{I_p})_{\pm}(x) := \lim_{h\to 0^+}(\mathcal{S}_{k,I_p}\varphi_{I_p})(x \pm h\nu(x)), \quad x \in I_p,$$

$$\lim_{h\to 0^+}\left(\frac{\partial}{\partial\nu}\mathcal{S}_{k,I_p}\varphi_{I_p}\right)_{\pm}(x) := \left(\nu\cdot\nabla\mathcal{S}_{k,I_p}\varphi_{I_p}\right)(x \pm h\nu(x)), \quad x \in I_p.$$

For $I_q \in \{\Gamma_R, \partial B_R^-, \widetilde{\Gamma}\}$ it is easy to see that $S_{k,I_p\to I_q} : L^2(I_p) \to H^1(I_q)$, $K'_{k,I_p\to I_q} : L^2(I_p) \to L^2(I_q)$ and $K'^{,re}_{k,I_p\to\partial B_R^-} : L^2(I_p) \to L^2(\partial B_R^-)$ are bounded operators.

(ii) Let $\varphi_{\widetilde{\Gamma}} \in H^{-1/2}(\widetilde{\Gamma})$. Then, from [44, Chapter 6] it follows that $\mathcal{S}_{k,\widetilde{\Gamma}}\varphi_{\widetilde{\Gamma}} \in H^1_{loc}(\mathbb{R}^2)$ and satisfies the Helmholtz equation (1.1) in $\mathbb{R}^2\backslash\overline{\widetilde{\Gamma}}$ as well as the jump relations (2.8) and (2.9) on the curve $I_p = \widetilde{\Gamma}$. Further, since $\widetilde{\Gamma}$ is a C^2-smooth curve, by [24] it is known that $S_{k,\widetilde{\Gamma}\to\widetilde{\Gamma}}$ and $K'_{k,\widetilde{\Gamma}\to\widetilde{\Gamma}}$ are compact operators from $H^{-1/2}(\widetilde{\Gamma})$ to $H^{-1/2}(\widetilde{\Gamma})$). Moreover, it can be seen that $K'_{k,\widetilde{\Gamma}\to\Gamma_R} : H^{-1/2}(\widetilde{\Gamma}) \to L^2(\Gamma_R)$ and $K'_{k,\widetilde{\Gamma}\to\partial B_R^-}, K'^{,re}_{k,\widetilde{\Gamma}\to\partial B_R^-} : H^{-1/2}(\widetilde{\Gamma}) \to L^2(\partial B_R^-))$ are bounded operators since the kernels of those operators are smooth functions.

We now derive the equivalent integral equation formulation for the Neumann problem (NP). Let u^s be the solution to the Neumann problem (NP). We now extend $u^s(x)$ into $\mathbb{R}^2_-\backslash\overline{B}_R$ by reflection, which we denote by $u^s(x)$ again, such that $u^s(x) = u^s(x^{re})$ for $x \in \mathbb{R}^2_-\backslash\overline{B}_R$. Then, from the reflection principle and the Neumann boundary condition $\partial u^s/\partial\nu = -(\partial u^i/\partial\nu + \partial u^r/\partial\nu) = 0$ on $\Gamma \setminus \overline{B}_R$ it follows that $u^s \in H^1_{loc}(\mathbb{R}^2\backslash\overline{D_R^-})$ and satisfies the Helmholtz equation (1.1) in $\mathbb{R}^2\backslash\overline{D_R^-}$. Following the idea in [8], we seek the solution u^s in the form

$$u^s(x) = \int_{\Gamma_R} G_k(x,y)\varphi_1(y)ds(y) + \int_{\partial B_R^-} G_k(x,y)\varphi_2(y)ds(y) + \int_{\widetilde{\Gamma}} G_k(x,y)\varphi_3(y)ds(y), \quad x \in \mathbb{R}^2\backslash(\partial D_R^- \cup \widetilde{\Gamma}), \tag{2.10}$$

with $\Phi = (\varphi_1,\varphi_2,\varphi_3)^T \in X := L^2(\Gamma_R)\times L^2(\partial B_R^-)\times H^{-\frac{1}{2}}(\widetilde{\Gamma})$ with the norm $\|\Phi\|_X := \|\varphi_1\|_{L^2(\Gamma_R)} + \|\varphi_2\|_{L^2(\partial B_R^-)} + \|\varphi_3\|_{H^{-1/2}(\widetilde{\Gamma})}$. We will prove that by choosing appropriate auxiliary curve $\widetilde{\Gamma}$ the Neumann problem (NP) can be reduced to an equivalent boundary integral equation which is uniquely solvable (see Theorem 2.4 and Remark 2.5 below).

Let ψ^{re} be a continuous mapping from ∂D_R^- to ∂D_R^+ such that

$$\psi^{re}(x) = \begin{cases} x, & x \in \Gamma_R, \\ x^{re}, & x \in \partial B_R^- \cup \{x_A, x_B\}. \end{cases}$$

Then, by the boundary condition (2.1) and the reflection principle, $u^s(x)$ satisfies

$$\frac{\partial u^s(x)}{\partial\nu(x)} = -\left(\frac{\partial u^i(x)}{\partial\nu(x)} + \frac{\partial u^r(x)}{\partial\nu(x)}\right) \quad \text{for } x \in \Gamma_R, \tag{2.11}$$

$$\frac{\partial u^s(x)}{\partial\nu(x)} - \frac{\partial u^s(\psi^{re}(x))}{\partial\nu(x^{re})} = 0 \quad \text{for } x \in \partial B_R^-. \tag{2.12}$$

We now impose the impedance boundary condition for u^s on the auxiliary curve $\widetilde{\Gamma}$:

$$\frac{\partial u^s(x)}{\partial\nu(x)} + i\rho u^s(x) = 0 \quad \text{for } x \in \widetilde{\Gamma}, \tag{2.13}$$

where ρ is a positive constant. Then the jump relations (see Remark 2.2) and boundary conditions (2.11)–(2.13) lead to the boundary integral equation

$$(I + A)\Phi = E, \tag{2.14}$$

where I is the identity operator and A, E are given by

$$A := (A_{ij})_{3\times 3} \tag{2.15}$$

with $A_{11} = -2K'_{k,\Gamma_R\to\Gamma_R}$, $A_{12} = -2K'_{k,\partial B_R^-\to\Gamma_R}$, $A_{13} = -2K'_{k,\widetilde{\Gamma}\to\Gamma_R}$, $A_{21} = -2(K'_{k,\Gamma_R\to\partial B_R^-} - K'^{,re}_{k,\Gamma_R\to\partial B_R^-})$, $A_{22} = -2(K'_{k,\partial B_R^-\to\partial B_R^-} - K'^{,re}_{k,\partial B_R^-\to\partial B_R^-})$, $A_{23} = -2(K'_{k,\widetilde{\Gamma}\to\partial B_R^-} - K'^{,re}_{k,\widetilde{\Gamma}\to\partial B_R^-})$, $A_{31} = -2(K'_{k,\Gamma_R\to\widetilde{\Gamma}} + i\rho S_{k,\Gamma_R\to\widetilde{\Gamma}})$, $A_{32} = -2(K'_{k,\partial B_R^-\to\widetilde{\Gamma}} + i\rho S_{k,\partial B_R^-\to\widetilde{\Gamma}})$, $A_{33} = -2(K'_{k,\widetilde{\Gamma}\to\widetilde{\Gamma}} + i\rho S_{k,\widetilde{\Gamma}\to\widetilde{\Gamma}})$, and

$$E := \begin{pmatrix} 2\left(\partial u^i/\partial\nu + \partial u^r/\partial\nu\right)\big|_{\Gamma_R} \\ 0 \\ 0 \end{pmatrix}. \tag{2.16}$$

Obviously, $E \in X$. Further, it is seen from Remark 2.2 that A is a bounded linear operator on X. Note that the purpose of imposing the impedance boundary condition (2.13) on u^s is to ensure uniqueness of solutions to the integral equation (2.14) (see the discussions in Step II of the proof of Theorem 2.4 for further details).

Conversely, we have the following result.

LEMMA 2.3. *Let u^s be given by* (2.10) *with $\Phi = (\varphi_1, \varphi_2, \varphi_3)^T \in X$ which is the solution of the boundary integral equation* (2.14) *with A and E defined in* (2.15) *and* (2.16)*, respectively. Then $u^s \in H^1_{loc}(\mathbb{R}^2\backslash\overline{D_R^-})$ and solves the Neumann problem* (NP).

Proof. By the fact that $\Phi = (\varphi_1, \varphi_2, \varphi_3)^T \in X$ and Remark 2.2, it is easy to see that u^s defined by (2.10) satisfies the Helmholtz equation (1.1) in $\mathbb{R}^2\backslash\overline{D_R^-}$ and the Sommerfeld radiation condition (1.3) and is in $H^1_{loc}(\mathbb{R}^2\backslash\overline{D_R^-})$. Further, by the integral equation $(I + A)\Phi = E$ and the jump relations of the single-layer potentials (see Remark 2.2), it follows that $\partial u^s(x)/\partial\nu(x) = -\partial u^i(x)/\partial\nu(x) - \partial u^r(x)/\partial\nu(x)$ for $x \in \Gamma_R$ and $\partial u^s(x)/\partial\nu(x) = \partial u^s(x^{re})/\partial\nu(x^{re})$ for $x \in \partial B_R^-$.

Let $w^s(x) = u^s(x^{re})$ for $x \in \mathbb{R}^2\backslash\overline{B}_R$. Then w^s satisfies the Helmholtz equation (1.1) in $\mathbb{R}^2\backslash\overline{B}_R$, the Sommerfeld radiation condition (1.3), and the condition $\partial w^s(x)/\partial\nu(x) = \partial u^s(x)/\partial\nu(x)$ for $x \in \partial B_R$. Further, it follows from the uniqueness of the exterior Neumann problem (see, e.g., [24, Chapter 3]) that $w^s = u^s$ in $\mathbb{R}^2\backslash\overline{B}_R$, which implies that $u^s(x) = u^s(x^{re})$ in $\mathbb{R}^2\backslash\overline{B}_R$. In particular, we obtain that $\partial u^s/\partial\nu = 0$ on $\Gamma\backslash\Gamma_R$. Therefore, we have $\partial u^s/\partial\nu = -(\partial u^i/\partial\nu + \partial u^r/\partial\nu)$ on Γ. The proof is thus complete. ∎

The following theorem gives the unique solvability of the integral equation $(I + A)\Phi = E$.

THEOREM 2.4. *Assume that k^2 is not a Dirichlet eigenvalue of $-\Delta$ in $\widetilde{D}$. Let A and E be given by* (2.15) *and* (2.16)*, respectively. Then the integral equation $(I + A)\Phi = E$ has a unique solution $\Phi = (\varphi_1, \varphi_2, \varphi_3)^T \in X$ with the estimate*

$$||\varphi_1||_{L^2(\Gamma_R)} + ||\varphi_2||_{L^2(\partial B_R^-)} + ||\varphi_3||_{H^{-1/2}(\widetilde{\Gamma})} \le C \left\| \frac{\partial u^i}{\partial\nu} + \frac{\partial u^r}{\partial\nu} \right\|_{L^2(\Gamma)}. \tag{2.17}$$

Proof. The proof is broken down into the following steps.

Step I. We show that $I + A$ is a Fredholm operator of index zero.

Step I.1. Define

$$M_0 := (M_{0ij})_{3\times 3} = \begin{pmatrix} -2K'_{0,\Gamma_R\to\Gamma_R} & -2K'_{0,\partial B_R^-\to\Gamma_R} & 0 \\ -2\left(K'_{0,\Gamma_R\to\partial B_R^-} - K'^{,re}_{0,\Gamma_R\to\partial B_R^-}\right) & -2\left(K'_{0,\partial B_R^-\to\partial B_R^-} - K'^{,re}_{0,\partial B_R^-\to\partial B_R^-}\right) & 0 \\ 0 & 0 & 0 \end{pmatrix}.$$

Then it follows from Remark 2.2 that M_0 is bounded in X. In addition, the kernels of $A_{ij} - M_{0ij}$, $i, j = 1, 2$, are bounded with the upper bound

$$C\left[\max\left(\ln\frac{1}{|x-y|}, 1\right) + \max\left(\ln\frac{1}{|\psi^{re}(x)-y|}, 1\right)\right]$$

for $x, y \in \partial D_R^-$ with $x \neq y$ and thus weakly singular since $|x-y| \le C|\psi^{re}(x)-y|$ for $x, y \in \partial D_R^-$. Therefore, $A_{ij} - M_{0ij}$, $i, j = 1, 2$, are compact. Further, the operators $A_{13}, A_{23}, A_{31}, A_{32}$ are compact since the kernels of those operators are smooth functions, and, by Remark 2.2, the operator A_{33} is also compact. Consequently, $A - M_0$ is compact in X.

For $z \in \mathbb{R}^2$ and $r \in \mathbb{R}$ define $B_r(z) := \{x \in \mathbb{R}^2 \mid |x-z| < r\}$. Obviously, we can choose a fixed $r_0 > 0$ such that for $z = x_A, x_B$, $B_r(z) \cap \Gamma_p = \emptyset$ and $\overline{B_r(x_A)} \cap \overline{B_r(x_B)} = \emptyset$ for $r \le r_0$. In the remaining part of the proof, we will choose $r \le r_0$. Now, choose a cut-off function $\psi_{r,z} \in C_0^\infty(\mathbb{R}^2)$ satisfying that $0 \le \psi_{r,z} \le 1$, $\psi_{r,z}(x) = 1$ in the region $0 \le |x-z| \le r/2$ and $\psi_{r,z}(x) = 0$ in the region $|x-z| \ge r$. Define $M_{0,r} : X \to X$ by $M_{0,r} := ((M_{0,r})_{ij})_{3\times 3}$ with

$$(M_{0,r})_{ij}\varphi_j := \begin{cases} \psi_{r,x_A}(M_0)_{ij}(\psi_{r,x_A}\varphi_j) + \psi_{r,x_B}(M_0)_{ij}(\psi_{r,x_B}\varphi_j), & i,j = 1,2, \\ 0 & \text{otherwise} \end{cases}$$

for any $\Phi = (\varphi_1, \varphi_2, \varphi_3)^T \in X$. Since the kernel of $M_0 - M_{0,r}$ vanishes in a neighborhood of (x_A, x_A) and (x_B, x_B), $M_0 - M_{0,r}$ is compact. Then the operator $A - M_{0,r} = (A - M_0) + (M_0 - M_{0,r})$ is compact from X into X.

Step I.2. We show that $||M_{0,r}||_{X\to X} < 1$ for a sufficiently small constant $r > 0$.

By the definition of $M_{0,r}$, we have that for any $\Phi = (\varphi_1, \varphi_2, \varphi_3)^T \in X$,

$$\begin{aligned} \|M_{0,r}\Phi\|_X &= \left\| \sum_{j=1}^{2} \left(\psi_{r,x_A}(M_0)_{1j}(\psi_{r,x_A}\varphi_j) + \psi_{r,x_B}(M_0)_{1j}(\psi_{r,x_B}\varphi_j)\right) \right\|_{L^2(\Gamma_R)} \\ &\quad + \left\| \sum_{j=1}^{2} \left(\psi_{r,x_A}(M_0)_{2j}(\psi_{r,x_A}\varphi_j) + \psi_{r,x_B}(M_0)_{2j}(\psi_{r,x_B}\varphi_j)\right) \right\|_{L^2(\partial B_R^-)} \\ &\le \sum_{j=1}^{2} \| \left(\psi_{r,x_A}(M_0)_{1j}(\psi_{r,x_A}\varphi_j) + \psi_{r,x_B}(M_0)_{1j}(\psi_{r,x_B}\varphi_j)\right) \|_{L^2(\Gamma_R)} \\ &\quad + \sum_{j=1}^{2} \| \left(\psi_{r,x_A}(M_0)_{2j}(\psi_{r,x_A}\varphi_j) + \psi_{r,x_B}(M_0)_{2j}(\psi_{r,x_B}\varphi_j)\right) \|_{L^2(\partial B_R^-)}. \end{aligned}$$

Recalling that $\overline{B_r(x_A)} \cap \overline{B_r(x_B)} = \emptyset$ and $\mathrm{supp}(\psi_{r,z}) \subset \overline{B_r(z)}$ for $z = x_A, x_B$, we find that

$$\begin{aligned}
&\|M_{0,r}\Phi\|_X \\
&\quad \le \sum_{j=1}^{2} \left(\|\psi_{r,x_A}(M_0)_{1j}(\psi_{r,x_A}\varphi_j)\|^2_{L^2(\Gamma_R)} + \|\psi_{r,x_B}(M_0)_{1j}(\psi_{r,x_B}\varphi_j)\|^2_{L^2(\Gamma_R)} \right)^{\frac{1}{2}} \\
&\qquad + \sum_{j=1}^{2} \left(\|\psi_{r,x_A}(M_0)_{2j}(\psi_{r,x_A}\varphi_j)\|^2_{L^2(\partial B_R^-)} + \|\psi_{r,x_B}(M_0)_{2j}(\psi_{r,x_B}\varphi_j)\|^2_{L^2(\partial B_R^-)} \right)^{\frac{1}{2}}.
\end{aligned}$$

We will estimate each term of the right-hand side of the above inequality. In doing so, the following inequality plays an essential role:

$$|\nu(x) \cdot (x-y)| \le C|x-y|^2 \tag{2.18}$$

for $x, y \in \Gamma_R$ or for $x \in \partial B_R$, $y \in \partial B_R^-$ (see [24, section 3.5]).

We first estimate the norm of $\psi_{r,z}(M_0)_{ij}(\psi_{r,z}\varphi_j)$, $i,j = 1,2$, with $z = x_A$ in the following four steps.

(i) For $\psi_{r,x_A}(M_0)_{11}(\psi_{r,x_A}\varphi_1)$ we have

$$\begin{aligned}
\psi_{r,x_A}(M_0)_{11}(\psi_{r,x_A}\varphi_1) &= -2\psi_{r,x_A} K'_{0,\Gamma_R\to\Gamma_R}(\psi_{r,x_A}\varphi_1) \\
&= -2\psi_{r,x_A}(x) \int_{\Gamma_R \cap B_r(x_A)} \frac{\partial G_0(x,y)}{\partial \nu(x)} \psi_{r,x_A}(y)\varphi_1(y) ds(y).
\end{aligned}$$

It then follows from (2.18) that

$$\begin{aligned}
&\|\psi_{r,x_A}(M_0)_{11}(\psi_{r,x_A}\varphi_1)\|^2_{L^2(\Gamma_R)} \\
&\qquad \le \|(M_0)_{11}\psi_{r,x_A}\varphi_1\|^2_{L^2(\Gamma_R\cap B_r(x_A))} \\
&\qquad = \int_{\Gamma_R\cap B_r(x_A)} \left(\int_{\Gamma_R\cap B_r(x_A)} 2\frac{\partial G_0(x,y)}{\partial \nu(x)} \psi_{r,x_A}(y)\varphi_1(y) ds(y) \right)^2 ds(x) \\
&\qquad \le C \int_{\Gamma_R\cap B_r(x_A)} \|\varphi_1\|^2_{L^2(\Gamma_R\cap B_r(x_A))} ds(x) \\
&\qquad \le Cr\|\varphi_1\|^2_{L^2(\Gamma_R\cap B_r(x_A))}. \qquad (2.19)
\end{aligned}$$

(ii) We estimate the norm of $\psi_{r,x_A}(M_0)_{12}(\psi_{r,x_A}\varphi_2)$. Since $x_A = (-R, 0)$, the curve $\Gamma_R \cap B_r(x_A)$ can be parameterized as $x(t) = (-R+t, 0)$, $t \in [0, r]$. Further, it is easily seen that $\partial B_R^- \cap \partial B_r(x_A) = (-\sqrt{R^2 - \tau_r^2}, -\tau_r)$ with $\tau_r := r\sqrt{4R^2 - r^2}/(2R)$. Thus $\partial B_R^- \cap B_r(x_A)$ can be parameterized as $y(\tau) = (y_1(\tau), y_2(\tau)) := (-\sqrt{R^2 - \tau^2}, -\tau)$, $\tau \in [0, r\sqrt{4R^2 - r^2}/(2R)]$. Then $y_1(0) = -R, y_1'(0) = 0$. Choose $\delta \in (0,1)$. Then there exists a $\tau(\delta) > 0$ such that $|y_1(\tau) - (-R)| \le \delta\tau$ and $|y_1'(\tau)| \le \delta$ for all $\tau \in [0, \tau(\delta)]$. Thus we have that for $t \in [0, r]$, $\tau \in [0, \tau(\delta)]$,

$$|y'(\tau)| = \sqrt{|y_1'(\tau)|^2 + |y_2'(\tau)|^2} \le \sqrt{1+\delta^2} \le 1 + \delta, \tag{2.20}$$

$$\begin{aligned}
|x(t) - y(\tau)|^2 &= (-R + t - y_1(\tau))^2 + \tau^2 \\
&\ge t^2 - 2t(y_1(\tau) + R) + \tau^2 \ge t^2 - \delta t^2 - \frac{1}{\delta}(y_1(\tau) + R)^2 + \tau^2 \\
&\ge (1-\delta)t^2 - \frac{1}{\delta}(\delta\tau)^2 + \tau^2 = (1-\delta)(t^2 + \tau^2). \qquad (2.21)
\end{aligned}$$

Further, from (2.21) it follows that

$$\frac{|y_2(\tau)|}{|x(t)-y(\tau)|^2} \le \frac{1}{1-\delta}\frac{\tau}{t^2+\tau^2}. \tag{2.22}$$

Now, choose $r > 0$ small enough so that $r\sqrt{4R^- r^2}/(2R) \le \min[\tau(\delta), 1]$ and $r \le \min[r_0, 1]$. Then, applying the parameterizations of $x(t)$ and $y(\tau)$, and using the inequalities (2.20) and (2.22), we obtain that

$$\begin{aligned}
&\|\psi_{r,x_A}(M_0)_{12}(\psi_{r,x_A}\varphi_2)\|^2_{L^2(\Gamma_R)} \\
&\quad\le \int_{\Gamma_R\cap B_r(x_A)} \left(\int_{\partial B_R^-\cap B_r(x_A)} 2\frac{\partial G_0(x,y)}{\partial \nu(x)}\psi_{r,x_A}(y)\varphi_2(y)ds(y)\right)^2 ds(x) \\
&\quad\le \int_0^r \left(2\int_0^{\frac{\sqrt{4R^2-r^2}}{2R}r} \left|\frac{\partial G_0(x,y)}{\partial \nu(x(t))}\right| \cdot |\varphi_2(y(\tau))| \cdot |y'(\tau)| d\tau\right)^2 |x'(t)|dt \\
&\quad\le \int_0^r \left(\frac{1}{\pi}\int_0^{\frac{\sqrt{4R^2-r^2}}{2R}r} \frac{|y_2(\tau)|}{|x(t)-y(\tau)|^2}|\varphi_2(y(\tau))| \cdot |y'(\tau)| d\tau\right)^2 |x'(t)|dt \\
&\quad\le \int_0^r \left(\frac{1+\delta}{1-\delta}\int_0^{\frac{\sqrt{4R^2-r^2}}{2R}r} \frac{\tau}{\pi(t^2+\tau^2)}|\varphi_2(y(\tau))| d\tau\right)^2 dt.
\end{aligned}$$

Let

$$\widetilde{\varphi}_2(\tau) = \begin{cases} \varphi_2(y(\tau)) & \text{if} \quad 0 \le \tau \le r\sqrt{4R^2-r^2}/(2R), \\ 0 & \text{if} \quad r\sqrt{4R^2-r^2}/(2R) < \tau \le 1. \end{cases}$$

Then

$$\|\psi_{r,x_A}(M_0)_{12}(\psi_{r,x_A}\varphi_2)\|_{L^2(\Gamma_R)} \le \frac{1+\delta}{1-\delta}\left(\int_0^1 \left(\int_0^1 \frac{\tau}{\pi(t^2+\tau^2)}|\widetilde{\varphi}_2(\tau)|d\tau\right)^2 dt\right)^{\frac{1}{2}}. \tag{2.23}$$

For any $v \in L^2(0,1)$, define the operator

$$(Rv)(t) := \int_0^1 \frac{t}{\pi(t^2+\tau^2)} v(\tau) d\tau.$$

From [12, Lemma 1] it is known that R is a linear bounded operator on $L^2(0,1)$ with the norm $\|R\|_{L^2(0,1)\to L^2(0,1)} \le \sin(\pi/4) = 1/\sqrt{2}$. Further, it is easy to see that

$$\left(\int_0^1 \left(\int_0^1 \frac{\tau}{\pi(t^2+\tau^2)}|\widetilde{\varphi}_2(\tau)|d\tau\right)^2 dt\right)^{\frac{1}{2}} = \|R^*|\widetilde{\varphi}_2|\|_{L^2(0,1)}.$$

It then follows by (2.23) and the fact that $\|R^*\|_{L^2(0,1)\to L^2(0,1)} = \|R\|_{L^2(0,1)\to L^2(0,1)}$ that

$$\|\psi_{r,x_A}(M_0)_{12}(\psi_{r,x_A}\varphi_2)\|_{L^2(\Gamma_R)} \le \frac{1+\delta}{1-\delta}\|R^*|\widetilde{\varphi}_2|\|_{L^2(0,1)} \le \frac{1+\delta}{1-\delta}\frac{1}{\sqrt{2}}\|\widetilde{\varphi}_2\|_{L^2(0,1)}. \tag{2.24}$$

Now, since $|y'(\tau)| = \sqrt{(y_1'(\tau))^2 + (y_2'(\tau))^2} \geq |y_2'(\tau)| = 1$ for $\tau \in [0, \tau(\delta)]$, we have

(2.25)
$$\|\varphi_2\|_{L^2(\partial B_R^- \cap B_r(x_A))} = \left(\int_0^{\frac{\sqrt{4R^2-r^2}}{2R} r} (\varphi_2(y(\tau)))^2 |y'(\tau)| d\tau \right)^{\frac{1}{2}} \geq \|\widetilde{\varphi}_2\|_{L^2(0,1)}.$$

It thus follows from (2.24) and (2.25) that

$$\|\psi_{r,x_A}(M_0)_{12}(\psi_{r,x_A}\varphi_2)\|_{L^2(\Gamma_R)} \leq \frac{1+\delta}{1-\delta}\frac{1}{\sqrt{2}}\|\varphi_2\|_{L^2(\partial B_R^- \cap B_r(x_A))}. \tag{2.26}$$

(iii) For $\psi_{r,x_A}(M_0)_{21}(\psi_{r,x_A}\varphi_1)$, we have

$$\begin{aligned}
&\psi_{r,x_A}(M_0)_{21}(\psi_{r,x_A}\varphi_1) \\
&\quad = -2\psi_{r,x_A}\left(K'_{0,\Gamma_R\to\partial B_R^-} - K'^{,re}_{0,\Gamma_R\to\partial B_R^-}\right)(\psi_{r,x_A}\varphi_1) \\
&\quad = -2\psi_{r,x_A}(x)\int_{\Gamma_R}\left(\frac{\partial G_0(x,y)}{\partial\nu(x)} - \frac{\partial G_0(x^{re},y)}{\partial\nu(x)}\right)\psi_{r,x_A}(y)\varphi_1(y)ds(y). \qquad (2.27)
\end{aligned}$$

It is easy to verify that for $y \in \Gamma_R \cap B_r(x_A)$ and $x \in \partial B_R^- \cap B_r(x_A)$,

$$\frac{\partial \ln|x-y|}{\partial\nu(x)} = \frac{\nu(x)\cdot(x_1-y_1,x_2)}{|x-y|^2}.$$

Then, by the definition of x^{re} and $\nu(x^{re})$ we have that for $y \in \Gamma_R \cap B_r(x_A)$ and $x \in \partial B_R^- \cap B_r(x_A)$,

$$\frac{\partial \ln|x-y|}{\partial\nu(x)} - \frac{\partial \ln|x^{re}-y|}{\partial\nu(x)} = 0.$$

Combining this with (2.27) implies that

$$\|\psi_{r,x_A}(M_0)_{21}(\psi_{r,x_A}\varphi_1)\|_{L^2(\partial B_R^-)} = 0. \tag{2.28}$$

(iv) With the inequality (2.18), the estimate of $\psi_{r,x_A}(M_0)_{22}(\psi_{r,x_A}\varphi_2)$ is similar to that of $\psi_{r,x_A}(M_0)_{11}(\psi_{r,x_A}\varphi_1)$, and so we have

$$\|\psi_{r,x_A}(M_0)_{22}(\psi_{r,x_A}\varphi_2)\|^2_{L^2(\Gamma_R)} \leq Cr\|\varphi_2\|^2_{L^2(\partial B_R^- \cap B_r(x_A))}. \tag{2.29}$$

The norm of $\psi_{r,z}(M_0)_{ij}(\psi_{r,z}\varphi_j)$, $i,j = 1,2$, with $z = x_B$ can be estimated similarly, and we have similar estimates as (2.19), (2.26), (2.28), and (2.29).

We are now ready to estimate the norm of $M_{0,r}\Phi$. For arbitrarily fixed $\delta \in (0,1)$, we obtain by combining the estimates obtained in (i)–(iv) that there exists a $r > 0$ small enough such that

$$\begin{aligned}
\|M_{0,r}\Phi\|_X^2 &\leq Cr\left(\|\varphi_1\|^2_{L^2(\Gamma_R\cap B_r(x_A))} + \|\varphi_1\|^2_{L^2(\Gamma_R\cap B_r(x_B))}\right) \\
&\quad + \left[Cr + \frac{1}{2}\left(\frac{1+\delta}{1-\delta}\right)^2\right]\left(\|\varphi_2\|^2_{L^2(\partial B_R^-\cap B_r(x_A))} + \|\varphi_2\|^2_{L^2(\partial B_R^-\cap B_r(x_B))}\right) \\
&\leq Cr\|\varphi_1\|^2_{L^2(\Gamma_R)} + \left[Cr + \frac{1}{2}\left(\frac{1+\delta}{1-\delta}\right)^2\right]\|\varphi_2\|^2_{L^2(\partial B_R^-)} \\
&\leq \left[Cr + \frac{1}{2}\left(\frac{1+\delta}{1-\delta}\right)^2\right]\|\Phi\|_X^2.
\end{aligned}$$

Fix $0 < \delta < (\sqrt{2}-1)/(\sqrt{2}+1)$ to obtain that $(1+\delta)/(1-\delta) < \sqrt{2}$, so we have $\|M_{0,r}\|_{X\to X} < 1$ for $r > 0$ small enough.

Now, since $\|M_{0,r}\|_{X\to X} < 1$ for $r > 0$ small enough, $I + M_{0,r}$ has a bounded inverse in X. Thus, and since $I + A = I + M_{0,r} + (A - M_0) + (M_0 - M_{0,r})$, we know by Steps I.1 and I.2 that $I + A$ is a Fredholm operator of index zero. The proof of Step I is thus complete.

Step II. We prove that $I + A$ is injective and thus invertible in X.

Let $(I+A)\Phi = 0$ for $\Phi = (\varphi_1, \varphi_2, \varphi_3)^T \in X$. Then it follows from Lemma 2.3 that the scattered field u^s, given by (2.10), satisfies the boundary condition $\partial u^s/\partial\nu = 0$ on Γ. By Theorem 2.1 and the unique continuation principle we have $u^s = 0$ in $\mathbb{R}^2\backslash\overline{D_R^-}$. Then, by the jump relations of the layer potentials (see Remark 2.2) one has

$$u_-^s = u_+^s = 0 \quad \text{on} \quad \partial D_R^-, \tag{2.30}$$

where u_-^s and u_+^s indicate the limits of u^s on ∂D_R^- from D_R^- and $\mathbb{R}^2_- \backslash \overline{D_R^-}$, respectively. The integral equation $(I+A)\Phi = 0$ implies the boundary condition $\partial u_+^s/\partial\nu + i\rho u_+^s = 0$ on $\widetilde{\Gamma}$. Thus u^s satisfies the mixed boundary value problem

$$\begin{cases} \Delta u^s + k^2 u^s = 0 & \text{in } D_R^-\backslash\overline{\widetilde{D}}, \\ u_-^s = 0 & \text{on } \partial D_R^-, \\ \dfrac{\partial u_+^s}{\partial\nu} + i\rho u_+^s = 0 & \text{on } \widetilde{\Gamma}. \end{cases} \tag{2.31}$$

Here, u_+^s in the third equation indicates the limit of u^s on $\widetilde{\Gamma}$ from $D_R^- \setminus \overline{\widetilde{D}}$. From (2.31) and Green's formula it follows that

$$\int_{D_R^-\backslash\overline{\widetilde{D}}} \left(|\nabla u^s|^2 - k^2|u^s|\right) ds = i\rho \int_{\widetilde{\Gamma}} |u_+^s|^2 ds.$$

Taking the imaginary part of the above equation gives that $u_+^s = 0$ on $\widetilde{\Gamma}$. This, together with the last equation in (2.31), implies that $\partial u_+^s/\partial\nu = 0$ on $\widetilde{\Gamma}$. Holmgren's uniqueness theorem then yields that $u^s = 0$ in $D_R^-\backslash\overline{\widetilde{D}}$.

By the jump relations of the layer potentials on ∂D_R^-, one has

$$-\varphi_1 = \frac{\partial u_+^s}{\partial\nu} - \frac{\partial u_-^s}{\partial\nu} = 0 \quad \text{on} \quad \Gamma_R,$$
$$-\varphi_2 = \frac{\partial u_+^s}{\partial\nu} - \frac{\partial u_-^s}{\partial\nu} = 0 \quad \text{on} \quad \partial B_R^-.$$

On the other hand, the jump relations of the layer potentials on $\widetilde{\Gamma}$ give

$$u_-^s = u_+^s = 0 \quad \text{on} \quad \widetilde{\Gamma}.$$

We then obtain that u^s satisfies the impedance problem in $\widetilde{D}$:

$$\begin{cases} \Delta u^s + k^2 u^s = 0 & \text{in } \widetilde{D}, \\ u_-^s = 0 & \text{on } \widetilde{\Gamma}. \end{cases}$$

Since k^2 is not a Dirichlet eigenvalue of $-\Delta$ in $\widetilde{D}$, we have $u^s = 0$ in $\widetilde{D}$. The jump relations of layer potentials on $\widetilde{\Gamma}$ again imply that

$$-\varphi_3 = \frac{\partial u_+^s}{\partial\nu} - \frac{\partial u_-^s}{\partial\nu} = 0 \quad \text{on} \quad \widetilde{\Gamma}.$$

Therefore, we have $\Phi = (\varphi_1, \varphi_2, \varphi_3)^T = 0$, yielding that $I + A$ is injective on X.

By Step I and the Fredholm alternative it follows that $I + A$ has a bounded inverse on X, and the estimate (2.17) is thus obtained. This completes the proof of the theorem. ∎

Remark 2.5. In Theorem 2.4, it is assumed that k^2 is not a Dirichlet eigenvalue of $-\Delta$ in $\widetilde{D}$. It should be noted that in numerical computation this assumption can be easily fulfilled. In fact, $\widetilde{D}$ can be chosen to be a ball of radius r. Then, by [24] (see the proof of Corollary 5.3 of [24]) we know that k^2 is not a Dirichlet eigenvalue of $-\Delta$ in $\widetilde{D}$ if and only if kr is not the zeros of the Bessel function J_n of order n for any integer n. In particular, if the radius r is chosen so that kr is smaller than the smallest zero of the Bessel function J_0, then k^2 is not a Dirichlet eigenvalue of $-\Delta$ in $\widetilde{D}$.

Remark 2.6. It should be remarked that the circle ∂B_R can be replaced by any closed smooth curve which is symmetric about the plane $x_2 = 0$. However, it is computationally simple and convenient to use the circle ∂B_R.

We now conclude the following result on the well-posedness of the problem (NP) by combining Lemma 2.3, Theorems 2.1 and 2.4, and the mapping properties of the single- and double-layer potentials in X.

THEOREM 2.7. *The problem* (NP) *has a unique solution* $u^s \in H^1_{loc}(D_+)$. *Further, for any* $R > 0$ *we have*

$$||u^s||_{H^1(D_R^+)} \leq C \left\| \frac{\partial u^i}{\partial \nu} + \frac{\partial u^r}{\partial \nu} \right\|_{L^2(\Gamma)}. \tag{2.32}$$

Remark 2.8. By the asymptotic behavior of the fundamental solution G_k (see, e.g., [24]) and the form (2.10) of the scattered field u^s, it is easy to know that u^s has the following asymptotic behavior at infinity:

$$u^s(x;d) = \frac{e^{ik|x|}}{\sqrt{|x|}} \left(u^\infty(\hat{x};d) + O\left(\frac{1}{|x|}\right)\right), \qquad |x| \to \infty,$$

uniformly for all observation directions $\hat{x} \in \mathbb{S}^1_+$. Here, the far-field pattern $u^\infty(\hat{x};d)$ is given by

$$u^\infty(\hat{x}) = S^\infty \Phi := \left(S^\infty_{k,\Gamma_R}\varphi_1\right)(\hat{x}) + \left(S^\infty_{k,\partial B_R^-}\varphi_2\right)(\hat{x}) + \left(S^\infty_{k,\widetilde{\Gamma}}\varphi_3\right)(\hat{x}), \tag{2.33}$$

which is an analytic function on the unit circle $\mathbb{S}^1$, where $\Phi = (\varphi_1, \varphi_2, \varphi_3)^T \in X$ is the unique solution of the integral equation $(I + A)\Phi = E$ with A and E given by (2.15) and (2.16), respectively.

Remark 2.9. We may seek the solution u^s in the form

$$u^s(x) = \int_{\Gamma_R} G_k(x,y)\varphi_1(y)ds(y) + \int_{\partial B_R^-} G_k(x,y)\varphi_2(y)ds(y), \quad x \in \mathbb{R}^2 \backslash \partial D_R^-, \tag{2.34}$$

with $\Phi = (\varphi_1, \varphi_2)^T \in L^2(\Gamma_R) \times L^2(\partial B_R^-)$. Then, by using the boundary conditions (2.11) and (2.12) and the jump relations of layer potentials, we obtain the boundary integral equation

$$(I + B)\Phi = E, \tag{2.35}$$

where $B := (B_{ij})_{2\times 2}$ with $B_{ij} = A_{ij}$, $i,j = 1,2$ and A_{ij} given in (2.15), and $E = (2(\partial u^i/\partial\nu + \partial u^r/\partial\nu)|_{\Gamma_R}, 0)^T$.

By a similar argument as those used in the proof of Theorem 2.4, we can prove that if k^2 is not a Dirichlet eigenvalue of $-\Delta$ in D_R^- then $I+B$ is boundedly invertible on $L^2(\Gamma_R)\times L^2(\partial B_R^-)$ and that if $\Phi = (\varphi_1,\varphi_2)^T$ is the unique solution to the integral equation (2.35) then the scattering field u^s in the form (2.34) solves the Neumann problem (NP). Again, by the asymptotic behavior of the fundamental solution G_k, the far-field pattern of the scattered field u^s in the form (2.34) is given by

$$u^\infty(\hat{x}) = \left(S^\infty_{k,\Gamma_R}\varphi_1\right)(\hat{x}) + \left(S^\infty_{k,\partial B_R^-}\varphi_2\right)(\hat{x}). \tag{2.36}$$

It is seen that the integral equation (2.35) does not involve the auxiliary curve $\widetilde{\Gamma}$ and is much simpler than the integral equation (2.14). In the numerical experiments for the inverse problem we will make use of the integral equation (2.35) and the far-field pattern (2.36) to solve the solution of the direct scattering problem in each iteration (see section 5 for details).

3. Numerical solution of the direct scattering problem.

3.1. The numerical algorithm. In this subsection, we develop a numerical algorithm to solve the direct scattering problem, employing the boundary integral equation (2.14). Note that the kernels of the integral operators in the integral equation (2.14) are hypersingular near the corners x_A and x_B of the curve ∂D_R^-, leading to difficulties in numerical computation. To deal with this issue, we make use of the RCIP method to solve the integral equation (2.14). The RCIP method was first proposed by Helsing to solve planar boundary value problems in the presence of various boundary singularities and has been successfully applied to many kinds of static problems in nonsmooth domains, including the Helmholtz equation (see [34, 35, 36, 37]). In what follows, we will present the steps of our numerical algorithm based on the idea in [36]. For more details and applications of the RCIP method, the reader is referred to [34, 35, 36] and the references therein.

For the integral equation (2.14), we rewrite A and Φ as follows:

$$A = \begin{pmatrix} \hat{A}_{11} & \hat{A}_{12} \\ \hat{A}_{21} & \hat{A}_{22} \end{pmatrix},\ \Phi = \begin{pmatrix} \hat{\varphi}_1 \\ \hat{\varphi}_2 \end{pmatrix}$$

with

$$\hat{A}_{11} := \begin{pmatrix} A_{11} & A_{12} \\ A_{21} & A_{22} \end{pmatrix},\ \hat{A}_{12} := \begin{pmatrix} A_{13} \\ A_{23} \end{pmatrix},\ \hat{A}_{21} := \begin{pmatrix} A_{31} & A_{32} \end{pmatrix},\ \hat{A}_{22} := A_{33},$$

$$\hat{\varphi}_1 := \begin{pmatrix} \varphi_1 \\ \varphi_2 \end{pmatrix},\ \hat{\varphi}_2 := \varphi_3.$$

It can be seen that $\hat{A}_{11}$ is the integral operator B on ∂D_R^- defined in (2.35) in Remark 2.9. By the definition of A_{ij}, $i,j = 1,2$, it is seen that the operator $\hat{A}_{11}$ has the form $(\hat{A}_{11}\hat{\varphi}_1)(x) = \int_{\partial D_R^-}\hat{A}_{11}(x,y)\hat{\varphi}_1(y)ds(y)$, $x\in\partial D_R^-$, where the kernel $\hat{A}_{11}(x,y)$ of the operator $\hat{A}_{11}$ is given as

$$\hat{A}_{11}(x,y) = \begin{cases} -2\dfrac{\partial G_k(x,y)}{\partial\nu(x)}, & x\in\Gamma_R, y\in\partial D_R^-, x\neq y, \\ -2\left[\dfrac{\partial G_k(x,y)}{\partial\nu(x)} - \dfrac{\partial G_k(x^{re},y)}{\partial\nu(x^{re})}\right], & x\in\partial B_R^-,\ y\in\partial D_R^-, x\neq y. \end{cases}$$

Split the kernel $\hat{A}_{11}(x,y)$ into two parts

$$\hat{A}_{11}(x,y) = \hat{A}^{\star}_{11}(x,y) + \hat{A}^{\circ}_{11}(x,y), \tag{3.1}$$

such that $\hat{A}^{\star}_{11}(x,y)$ is zero except when both x and y are close enough to the same corner of ∂D_R^-. Thus $\hat{A}^{\circ}_{11}(x,y)$ is zero when x,y are close enough to the same corner of ∂D_R^-. Following the kernel split (3.1), we have the corresponding operator split

$$\hat{A}_{11} = \hat{A}^{\star}_{11} + \hat{A}^{\circ}_{11},$$

where $\hat{A}^{\circ}_{11}$ is a compact operator. Arguing similarly as in the proof of the fact that $||M_{0,r}||_{X\to X} < 1$ for a sufficiently small constant $r > 0$ in Step I.2 of the proof of Theorem 2.4, we can prove that $\|\hat{A}^{\star}_{11}\| < 1$ if, in the split of $\hat{A}_{11}$ above, $\hat{A}^{\star}_{11}(x,y)$ is zero except when both x and y are close enough to the same corner of ∂D_R^-, and so $(I + \hat{A}^{\star}_{11})^{-1}$ exists. By the variable substitution

$$\Phi = \begin{pmatrix} (I+\hat{A}^{\star}_{11})^{-1} & 0 \\ 0 & I \end{pmatrix} \widetilde{\Phi}, \qquad \widetilde{\Phi} := \begin{pmatrix} \widetilde{\varphi}_1 \\ \widetilde{\varphi}_2 \end{pmatrix},$$

the integral equation (2.14) is rewritten as a right preconditioned integral equation

$$\widetilde{\Phi}(x) + \begin{pmatrix} \hat{A}^{\circ}_{11} & \hat{A}_{12} \\ \hat{A}_{21} & \hat{A}_{22} \end{pmatrix} \begin{pmatrix} (I+\hat{A}^{\star}_{11})^{-1} & 0 \\ 0 & I \end{pmatrix} \widetilde{\Phi}(x) = E(x). \tag{3.2}$$

To discretize the integral equation (3.2) we need two different meshes: a coarse mesh and a fine mesh. For the coarse mesh, we divide each smooth curve $I_p \in \{\Gamma_R, \partial B_R^-, \widetilde{\Gamma}\}$ into n_{pan} panels which have approximately equal length. The fine mesh is constructed around the corner x_z from the coarse one by halving the two panels around the corner x_z each time and repeatedly n_{sub} times, $z = A, B$. Thus, for the curves ∂D_R^- and $\widetilde{\Gamma}$, there are totally $3n_{pan}$ panels on the coarse mesh and $3n_{pan} + 4n_{sub}$ panels on the fine mesh. For the geometry of the coarse and fine meshes, see Figure 3.1.

With these two meshes, the integral equation (3.2) can be discretized by using a Nyström scheme based on the composite 16-point Gauss–Legendre quadrature (see [34, section 2]). The quantities $\widetilde{\Phi}, \hat{A}^{\circ}_{11}, \hat{A}_{12}, \hat{A}_{21}, \hat{A}_{22}$ are simply discretized on the

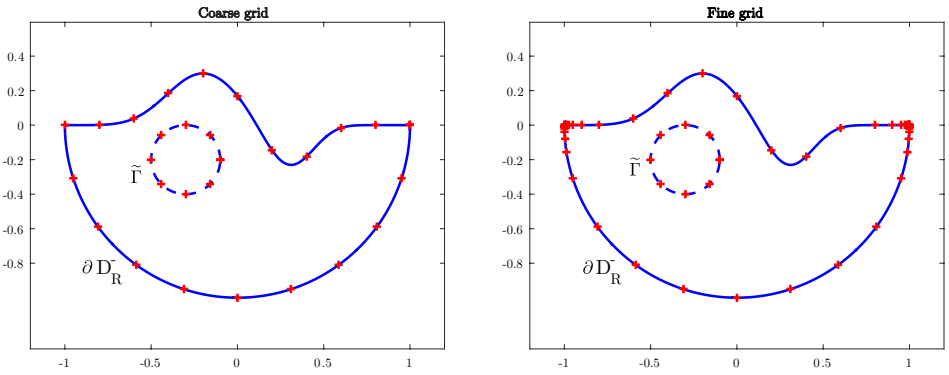

FIG. 3.1. *Geometry of the coarse and fine meshes.*

coarse mesh. Only the operator $(I + \hat{A}_{11}^{\star})^{-1}$ needs to be discretized on the fine mesh to get an accurate approximation. Then the discretized version of the integral equation (3.2) can be obtained as follows:

$$\left[\mathbf{I}_{\mathrm{coa}} + \begin{pmatrix} \hat{\mathbf{A}}_{11,\mathrm{coa}}^{\circ} & \hat{\mathbf{A}}_{12,\mathrm{coa}} \\ \hat{\mathbf{A}}_{21,\mathrm{coa}} & \hat{\mathbf{A}}_{22,\mathrm{coa}} \end{pmatrix} \begin{pmatrix} \mathbf{R} & \mathbf{0} \\ \mathbf{0} & \mathbf{I}_{\mathrm{coa}} \end{pmatrix}\right] \widetilde{\mathbf{\Phi}}_{\mathrm{coa}} = \mathbf{E}_{\mathrm{coa}}, \tag{3.3}$$

where $\widetilde{\mathbf{\Phi}}_{\mathrm{coa}}, \hat{\mathbf{A}}_{11,\mathrm{coa}}^{\circ}, \hat{\mathbf{A}}_{12,\mathrm{coa}}$, $\hat{\mathbf{A}}_{21,coa}, \hat{\mathbf{A}}_{22,coa}$ are the discretized matrixes of $\widetilde{\Phi}$, $\hat{A}_{11}^{\circ}$, $\hat{A}_{12}$, $\hat{A}_{21}$, $\hat{A}_{22}$, respectively, and $\mathbf{R}$ is called the compressed weighted inverse matrix and given by

$$\mathbf{R} = \mathbf{P}_{\mathrm{W}}^{\mathrm{T}} (\mathbf{I}_{\mathrm{fin}} + \hat{\mathbf{A}}_{11,\mathrm{fin}}^{\star})^{-1} \mathbf{P}.$$

Here, the subscript "coa" indicates the grid on the coarse mesh and the subscript "fin" indicates the grid on the fine mesh. The prolongation matrix $\mathbf{P}$ performs a polynomial interpolation from the coarse grid to the fine grid and $\mathbf{P}_{\mathrm{W}}^{\mathrm{T}}$ is the transpose of a weighted prolongation matrix (see [35, section 6]). Note that $\mathbf{R}$ depends on the fine mesh but can be easily computed by fast and stable recursion (see sections 7, 8, 12, and 13 in [35]).

By solving the linear equation (3.3), we get the unknown $\widetilde{\mathbf{\Phi}}_{\mathrm{coa}}$. Finally, the far-field pattern defined in (2.33) can be approximated as follows:

$$u^{\infty} \backsimeq \mathbf{S}_{\mathrm{coa}}^{\infty} \begin{pmatrix} \mathbf{R} & \mathbf{0} \\ \mathbf{0} & \mathbf{I}_{\mathrm{coa}} \end{pmatrix} \widetilde{\mathbf{\Phi}}_{\mathrm{coa}},$$

where $\mathbf{S}_{\mathrm{coa}}^{\infty}$ is the discretized matrix of S^{∞} on the coarse mesh of also using the composite 16-point Gauss–Legendre quadrature.

3.2. Numerical experiments. In this section, a numerical experiment is carried out to illustrate the performance of the algorithm proposed in section 3.1. We consider the locally rough surface Γ with

$$h(x_1) = \begin{cases} \exp\left[16/(25x_1^2 - 16)\right] \left[0.5 + 0.1\sin(16\pi x_1)\right], & |x_1| < 4/5, \\ 0, & |x_1| \geq 4/5. \end{cases}$$

Generally speaking, there is no exact solution of the scattering problem (NP) when the incident field is given by an incident plane wave. However, in some special cases, we can find a solution of the scattering problem (NP) which has an explicit expression. In this example, we choose $y = (-0.1, 0.1)$ and let $u^s(x; y)$ be the solution to the scattering problem (NP) with the boundary data $f = f(x; y) := -\partial G_k(x, y)/\partial\nu(x) - \partial G_k(x, y^{re})/\partial\nu(x)$ on $x \in \Gamma$, where $y^{re} = (-0.1, -0.1)$. Then it is easy to see that $y, y^{re} \in D_-$ (see Figure 3.2), implying that $-[G_k(x, y) + G_k(x, y^{re})]$ satisfies the Helmholtz equation (1.1) in D_+. Further, it can be seen that $G_k(x, y)$ and $G_k(x, y^{re})$ satisfy the radiation condition (1.3) and $f(x; y)$ has a compact support on Γ. Thus, by the uniqueness result for the scattering problem (NP) we have that the scattered field $u^s(x; y) = -G_k(x, y) - G_k(x, y^{re})$, $x \in D_+$. Thus it follows from the asymptotic behavior of G_k that the far-field pattern $u^{\infty}(\hat{x}; y)$ of the scattered field $u^s(x; y)$ is given by

$$u^{\infty}(\hat{x}; y) = -\frac{e^{i\pi/4}}{\sqrt{8\pi k}} \left(e^{-ik\hat{x}\cdot y} + e^{-ik\hat{x}\cdot y^{re}}\right),$$

which has an explicit expression and can be accurately computed.

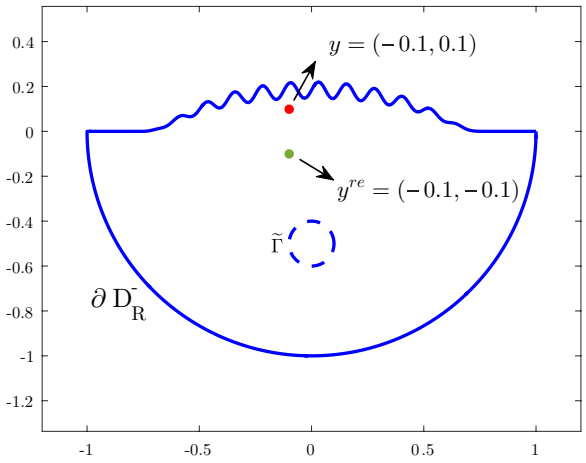

FIG. 3.2. *Geometry of the problem.*

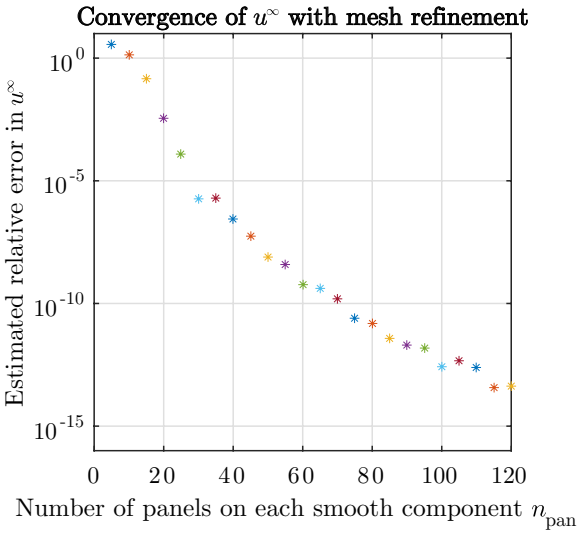

FIG. 3.3. *The relative error* $|u^\infty(\hat{x}; y) - u^\infty_{app}(\hat{x}; y)|/|u^\infty(\hat{x}; y)|$ *of the far-field pattern with* $n_{pan} = 5N$, $N = 1, 2, 3, \ldots, 24$, *respectively.*

We now compute the approximated value $u^\infty_{app}(\hat{x}; y)$ of the far-field pattern $u^\infty(\hat{x}; y)$, using the RCIP method proposed in section 3.1 with the following parameters.

(1) We choose $R = 1$, the wave number $k = 100$, and the observation direction $\hat{x} = (\cos(2\pi/3), \sin(2\pi/3))$.

(2) The auxiliary curve $\widetilde{\Gamma}$ is taken to be a disk of radius $r = 0.1$ and centered at $[0, -0.5]$. By Remark 2.5, it is valid to use the integral equation (2.14) to solve the Neumann problem (NP).

(3) The parameter ρ in the boundary condition (2.13) is chosen as $\rho = 1$.

(4) For the coarse mesh, we choose the number of panels on each smooth component to be $n_{pan} = 5N$ with $N = 1, 2, 3, \ldots, 24$, while, for the fine mesh, we choose the number of subdivisions to be $n_{sub} = 30$.

For the geometry of the problem, see Figure 3.2.

Figure 3.3 shows the relative error $|u^\infty(\hat{x};y)-u^\infty_{app}(\hat{x};y)|/|u^\infty(\hat{x};y)|$ of the far-field pattern with $n_{pan}=5N$, $N=1,2,3,\ldots,24$, respectively. It can be seen in Figure 3.3 that the RCIP method is very stable and capable of producing an accurate value of the far-field pattern if the parameter n_{pan} is large enough.

4. Uniqueness of the inverse problem. In this section, we establish uniqueness in the inverse scattering problem of reconstructing the locally rough surface from the far-field pattern associated with the incident plane wave at a fixed wave number $k>0$. Precisely, we will prove that the locally rough surface can be uniquely determined by the far-field patterns $u^\infty(\hat{x};d)$ for all $\hat{x}\in\mathbb{S}^1_+$, $d\in\mathbb{S}^1_-$ at a fixed wave number $k>0$. Our proof follows the idea in [24]. We now state the following lemma, which can be seen as an extension of Rellich's lemma for the case of bounded obstacles (see, e.g., [24, Lemma 2.12]).

LEMMA 4.1. *Assume that $u^s\in H^1_{loc}(\mathbb{R}^2_+\backslash\overline{B}_R)$ satisfies the Helmholtz equation (1.1) in $\mathbb{R}^2_+\backslash\overline{B}_R$, the Sommerfeld radiation condition (1.3), and the Neumann boundary condition $\partial u^s/\partial\nu=0$ on $\Gamma\backslash\overline{\Gamma}_R$. Assume further that the far-field pattern u^∞ of the scattering solution u^s vanishes on $\mathbb{S}^1_+$. Then u^s vanishes in $\mathbb{R}^2_+\backslash\overline{B}_R$.*

Proof. We extend u^s to $\mathbb{R}^2\backslash\overline{B}_R$ by reflection, which is denoted by u^s again, such that $u^s(x)=u^s(x^{re})$ in $\mathbb{R}^2_-\backslash\overline{B}_R$, where x^{re} is defined in section 2. Then, by reflection u^s satisfies the Helmholtz equation (1.1) in $\mathbb{R}^2\backslash\overline{B}_R$ and the Sommerfeld radiation condition (1.3) uniformly for all directions $\hat{x}=x/|x|$ with $x\in\mathbb{R}^2\backslash\overline{B}_R$. Further, the far-field pattern u^∞ of the scattering solution u^s vanishes on $\mathbb{S}^1$. Then, by Theorem 2.13 in [24] we obtain that u^s vanishes in $\mathbb{R}^2\backslash\overline{B}_R$, which completes the proof. ∎

To prove the uniqueness result for the inverse scattering problem, we consider the following boundary problem: for a given $y\in D_+$ find $v(x;y)$ such that

$$\Delta_x v(x;y)+k^2v(x;y)=-\delta(x-y) \quad \text{in } D_+, \tag{4.1}$$

$$\frac{\partial v}{\partial\nu}=0 \quad \text{on } \Gamma, \tag{4.2}$$

$$\lim_{r\to\infty} r^{\frac{1}{2}}\left(\frac{\partial v}{\partial r}-ikv\right)=0, \quad r=|x|, \quad x\in D_+. \tag{4.3}$$

From [2, Theorem 4.1] it can be seen that the problem (4.1)–(4.3) is well-posed. Then, the function $v(x;y)$ with $x,y\in D_+$ and $x\neq y$ can be viewed as the fundamental solution of the Helmholtz equation in D_+ with the Neumann condition on Γ. Define $v^s(x;y):=v(x;y)-G_k(x,y)$. Then it follows that for fixed $y\in D_+$, $v^s(x;y)$ satisfies the Helmholtz equation $\Delta v^s+k^2v^s=0$ in D_+, and so $v^s(x;y)$ is analytic in $x\in D_+$. Similarly as in the discussions in section 2, the Sommerfeld radiation condition (4.3) implies that $v(x;y)$ has the asymptotic behavior at infinity:

$$v(x;y)=\frac{e^{ik|x|}}{\sqrt{|x|}}\left(v^\infty(\hat{x};y)+O\left(\frac{1}{|x|}\right)\right), \qquad |x|\to\infty,$$

uniformly for all directions $\hat{x}=x/|x|\in\mathbb{S}^1_+$, where $v^\infty(\hat{x};y)$ denotes the far-field pattern of $v(x;y)$. Now, let $u^s(x;d)$ be the scattering solution generated by the incident plane wave $u^i(x;d)=\exp(ikd\cdot x)$ with the incident direction $d\in\mathbb{S}^1_-$, and so, $u(x;d)=u^i(x;d)+u^r(x;d)+u^s(x;d)$ is the total field. Then we have the following mixed reciprocity relation.

LEMMA 4.2. *$v^\infty(d;y)=\gamma u(y;-d)$ for all $y \in D_+$, $d \in \mathbb{S}^1_+$, where $\gamma=e^{i\pi/4}/\sqrt{8k\pi}$.*

Proof. Without loss of generality, we may assume that $y \in D_R^+$. Then, for $d \in \mathbb{S}^1_+$ and $\varepsilon > 0$ small enough we derive by Green's second theorem that

$$\begin{aligned}
&\int_{\partial B_R^+} \left[v(x;y)\frac{\partial u(x;-d)}{\partial \nu(x)} - u(x;-d)\frac{\partial v(x;y)}{\partial \nu(x)} \right] ds(x) \\
&\quad + \int_{|x-y|=\varepsilon} \left[v(x;y)\frac{\partial u(x;-d)}{\partial \nu(x)} - u(x;-d)\frac{\partial v(x;y)}{\partial \nu(x)} \right] ds(x) \\
&\quad = \int_{\Gamma_R} \left[v(x;y)\frac{\partial u(x;-d)}{\partial \nu(x)} - u(x;-d)\frac{\partial v(x;y)}{\partial \nu(x)} \right] ds(x) = 0, \qquad (4.4)
\end{aligned}$$

where ν is the unit normal on ∂B_R^+ pointing into $\mathbb{R}^2_+ \setminus \overline{D_R^+}$, on Γ_R directing into D_+, and on $\{x \in \mathbb{R}^2 : |x-y| = \varepsilon\}$ directing into $\{x \in \mathbb{R}^2 : |x-y| \le \varepsilon\}$, and the Neumann boundary condition on Γ_R of $v(x;y)$ and $u(x;-d)$ has been used to get the last equality.

Since $v^s(x;y)$ is analytic in the ball $\{x \in \mathbb{R}^2 : |x-y| \le \varepsilon\}$, by the singularity at $x = y$ of $G_k(x,y)$ and its derivative (see section 3.4 of [24]) we obtain that

$$-u(y;-d) = \lim_{\varepsilon \to 0} \int_{|x-y|=\varepsilon} \left[v(x;y)\frac{\partial u(x;-d)}{\partial \nu(x)} - u(x;-d)\frac{\partial v(x;y)}{\partial \nu(x)} \right] ds(x). \qquad (4.5)$$

On the other hand, we extend $v(x;y)$, $u^s(x;-d)$ into $\mathbb{R}^2_- \setminus \overline{B}_R$ by reflection, which are denoted again by $v(x;y)$, $u^s(x;-d)$, respectively, such that $v(x;y) = v(x^{re};y)$, $u^s(x;-d) = u^s(x^{re};-d)$ for $x \in \mathbb{R}^2_- \setminus \overline{B}_R$. Then, by the reflection principle $v(x;y)$, $u^s(x;-d)$ satisfy the Helmholtz equation (1.1) in $\mathbb{R}^2 \setminus \overline{B}_R$ and the Sommerfeld radiation condition (1.3) uniformly for all direction $\hat{x} = x/|x|$ with $x \in \mathbb{R}^2 \setminus \overline{B}_R$. Thus, by using the Sommerfeld radiation condition (1.3) for $v(x;y)$ and $u^s(x;-d)$ with $x \in \mathbb{R}^2 \setminus \overline{B}_R$, we derive immediately that

$$\begin{aligned}
0 &= \int_{\partial B_R} \left[v(x;y)\frac{\partial u^s(x;-d)}{\partial \nu(x)} - u^s(x;-d)\frac{\partial v(x;y)}{\partial \nu(x)} \right] ds(x) \\
&= 2\int_{\partial B_R^+} \left[v(x;y)\frac{\partial u^s(x;-d)}{\partial \nu(x)} - u^s(x;-d)\frac{\partial v(x;y)}{\partial \nu(x)} \right] ds(x). \qquad (4.6)
\end{aligned}$$

And, by using the formula (3.87) in [24] we further have

$$\begin{aligned}
v^\infty(d;y) &= \gamma \int_{\partial B_R} \left[v(x;y)\frac{\partial u^i(x;-d)}{\partial \nu(x)} - u^i(x;-d)\frac{\partial v(x;y)}{\partial \nu(x)} \right] ds(x) \\
&= \gamma \int_{\partial B_R^+} \left[v(x;y) \left[\frac{\partial u^i(x;-d)}{\partial \nu(x)} + \frac{\partial u^r(x;-d)}{\partial \nu(x)} \right] \right] ds(x) \\
&\quad - \gamma \int_{\partial B_R^+} \left[\left[u^i(x;-d) + u^r(x;-d) \right] \frac{\partial v(x;y)}{\partial \nu(x)} \right] ds(x), \qquad (4.7)
\end{aligned}$$

where we have used the fact that $u^i(x^e;-d) = u^r(x;-d)$ to get the second equality. Letting $\varepsilon \to 0$ in (4.4), using (4.5), (4.6), and (4.7), and noting that $u(x;d) = u^i(x;d) + u^r(x;d) + u^s(x;d)$ give the required result. This completes the proof. ∎

We are now ready to prove the following uniqueness theorem.

THEOREM 4.3. *Assume that $u_1^\infty(\hat{x};d)$ and $u_2^\infty(\hat{x};d)$ are the far-field patterns of the scattering solutions for the locally rough surfaces Γ_1 and Γ_2, respectively, corresponding to the same incident wave field $u^i(x;d)=\exp(ikd\cdot x)$. If $u_1^\infty(\hat{x};d)=u_2^\infty(\hat{x};d)$ for all $\hat{x}\in\mathbb{S}_+^1$ and $d\in\mathbb{S}_-^1$ with a fixed wave number $k>0$, then $\Gamma_1=\Gamma_2$.*

Proof. Denote by D_{l+} and D_{l-} the unbounded domains above and below the locally rough surface Γ_l, respectively, $l=1,2$. Suppose $D_{1+}\neq D_{2+}$. Without loss of generality, we may assume that there exists $z\in\Gamma_1\cap D_{2+}$ such that $\overline{B_h(z)}\subset D_{2+}$ for $h>0$ small enough, where $B_h(z):=\{x\in\mathbb{R}^2:|x-z|<h\}$. Define $z_j=z+(h/j)\nu(z)$, $j\in\mathbb{N}$, where $\nu(z)$ is the unit normal at $z\in\Gamma_1$ directed into D_{1+}.

Let $\mathcal{G}$ be the unbounded connected part of $D_{1+}\cap D_{2+}$. Denote by $\Gamma_{l,p}$ the local perturbation part of Γ_l, $l=1,2$, and assume that $\Gamma_{l,p}\subset B_R$ for some large enough $R>0$, $l=1,2$. Since $u_1^\infty(\hat{x};d)=u_2^\infty(\hat{x};d)$ for all $\hat{x}\in\mathbb{S}_+^1$ and $d\in\mathbb{S}_-^1$, and by Lemma 4.1, we have that $u_1^s(x;d)=u_2^s(x;d)$ for all $x\in\mathbb{R}_+^2\backslash\overline{B}_R$ and $d\in\mathbb{S}_-^1$. By the unique continuation principle it then follows that $u_1^s(x;d)=u_2^s(x;d)$ for all $x\in\mathcal{G}$ and $d\in\mathbb{S}_-^1$, and so $u_1(x;d)=u_2(x;d)$ for all $x\in\mathcal{G}$ and $d\in\mathbb{S}_-^1$. Let $v_l(x;y),x,y\in D_{l+},x\neq y$ $(l=1,2)$ be the solution of the problem (4.1)–(4.3) associated with the unbounded domain D_{l+} and let the locally rough surface Γ_l, $v_l^\infty(\hat{x};y)$ be the far-field pattern of $v_l(x;y)$ and $v_l^s(x;y):=v_l(x;y)-G_k(x,y)$. Then, by Lemma 4.2 we have $v_1^\infty(d;y)=v_2^\infty(d;y)$ for all $d\in\mathbb{S}_+^1$ and $y\in\mathcal{G}$. By Lemma 4.1 and the unique continuation principle again we obtain that $v_1(x;y)=v_2(x;y)$ for all $x,y\in\mathcal{G}$ with $x\neq y$ and thus $v_1^s(x;y)=v_2^s(x;y)$ for all $x,y\in\mathcal{G}$ with $x\neq y$. This, together with the continuity of $v_l^s,l=1,2$, yields that $v_1^s(x;y)=v_2^s(x;y)$ for all $x,y\in\mathcal{G}$. In particular, $v_1^s(x;z_j)=v_2^s(x;z_j)$, $j\in\mathbb{N}$, for all $x\in\mathcal{G}$.

Define $d(z_j,\Gamma_2):=\inf_{x\in\Gamma_2}|z_j-x|$, $j\in\mathbb{N}$. In view of the fact that $d(z_j,\Gamma_2)\geq\varepsilon_0>0$ with ε_0 independent of $j=1,2,\ldots$, by the well-posedness of the problem (4.1)–(4.3), we have that $\|\partial v_2^s(\cdot;z_j)/\partial\nu\|_{H^{1/2}(\Gamma_1\cap B_h(z))}\leq C$ with C independent of $j=1,2,\ldots$. On the other hand, by the boundary condition on Γ_1 we see that

$$\begin{aligned}\lim_{j\to\infty}\left\|\frac{\partial v_2^s(\cdot;z_j)}{\partial\nu}\right\|_{H^{1/2}(\Gamma_1\cap B_h(z))}&=\lim_{j\to\infty}\left\|\frac{\partial v_1^s(\cdot;z_j)}{\partial\nu}\right\|_{H^{1/2}(\Gamma_1\cap B_h(z))}\\&=\lim_{j\to\infty}\left\|\frac{\partial G_k(\cdot,z_j)}{\partial\nu}\right\|_{H^{1/2}(\Gamma_1\cap B_h(z))}=\infty.\end{aligned}$$

This is a contradiction, and thus $\Gamma_1=\Gamma_2$. The proof is then completed. ∎

5. Numerical solution of the inverse problem. In this section, we develop an inversion algorithm to solve the inverse problem numerically: given the far-field pattern u^∞ of the scattering solution u^s to the scattering problem (1.1)–(1.3) (or the problem (NP)) associated with a finite number of incident plane waves u^i with multiple wave numbers k (or multiple frequencies ω), we determine the unknown locally rough surface Γ (or the unknown surface profile h which describes the locally rough surface Γ). In particular, we propose a Newton-type reconstruction algorithm with multifrequency data for this inverse problem and conduct numerical experiments to demonstrate the effectiveness of the reconstruction algorithm.

5.1. Reconstruction algorithm with multifrequency data. We begin by introducing some notation. Given the incident plane wave $u_k^i(x;d)=e^{ikx\cdot d}$ with $d\in\mathbb{S}_-^1$, let u_k^s be the solution of the scattering problem (1.1)–(1.3) with respect to the surface profile function h characterizing the locally rough surface Γ. Assume that $u_k^\infty(\hat{x};d)$ is the far-field pattern of the scattering solution u_k^s. Define $C_{0,R}^2(\mathbb{R}):=\{h\in$

$C^2(\mathbb{R}) : \mathrm{supp}(h) \subset (-R, R)\}$ and define the far-field operator $F_{d,k} : C^2_{0,R}(\mathbb{R}) \to L^2(\mathbb{S}^1_+)$, which maps the function h to $u^\infty_k(\hat{x}; d)$, by

$$(F_{d,k}[h])(\hat{x}) = u^\infty_k(\hat{x}; d), \quad \hat{x} \in \mathbb{S}^1_+. \tag{5.1}$$

Here, we use the subscript k to indicate the dependence of u^i_k, u^s_k, u^∞_k, and $F_{d,k}$ on the wave number k.

Our reconstruction algorithm consists in solving the nonlinear and ill-posed equation (5.1) for the unknown function h using the Newton-type iterative method. To this end, we need to investigate the Fréchet differentiability of $F_{d,k}$ at h. Let $\triangle h \in C^2_{0,R}(\mathbb{R})$ be a small perturbation and let $\Gamma_{\triangle h} := \{(x_1, h(x) + \triangle h(x)) : x_1 \in \mathbb{R}\}$ denote the corresponding locally rough surface characterized by $h(x) + \triangle h(x)$. Then $F_{d,k}$ is called Fréchet differentiable at h if there exists a linear bounded operator $F'_{d,k} : C^2_{0,R}(\mathbb{R}) \to L^2(\mathbb{S}^1_+)$ such that

$$\left\| F_{d,k}[h + \triangle h] - F_{d,k}[h] - F'_{d,k}[h; \triangle h] \right\|_{L^2(\mathbb{S}^1_+)} = o\left(\|\triangle h\|_{C^2(\mathbb{R})} \right).$$

Throughout this paper we assume that the local perturbation $\Gamma_p \subset B_R$. Thus, in the inverse problem, we fix R and only consider the Fréchet differentiability of $F_{d,k}$ in the space $C^2_{0,R}(\mathbb{R})$.

For the Fréchet differentiability of $F_{d,k}$, we have the following theorem.

THEOREM 5.1. *Let $u(x; d) = u^i(x; d) + u^r(x; d) + u^s(x; d)$, where u^s solves the problem* (NP) *with the boundary data $f = -(\partial u^i/\partial\nu + \partial u^r/\partial\nu)$. If $h \in C^2_{0,R}(\mathbb{R})$, then $F_{d,k}$ is Fréchet differentiable at h with the derivative given by $F'_{d,k}[h; \triangle h] = (u')^\infty$ for $\triangle h \in C^2_{0,R}(\mathbb{R})$. Here, $(u')^\infty$ is the far-field pattern of u' which solves the problem* (NP) *with the boundary data $f = (d/ds)[(\nu_2 \triangle h)(du/ds)] + k^2(\nu_2 \triangle h)u$, where d/ds is the derivative with respect to the arc length and ν_2 is the second component of the unit normal vector ν on Γ directed into the unbounded domain D_+.*

Proof. The proof is similar to that of [2, Theorem 4.3], where the Fréchet derivative of $F_{d,k}$ is derived for the case of cavity problems with a Neumann boundary condition by using an variational method. ∎

With the aid of the Fréchet derivative of the far-field operator $F_{d,k}$, we are now ready to describe the Newton-type iteration method for solving the inverse problem. Let $d_l \in \mathbb{S}^1_-,\ l = 1, 2, \ldots, n_d$, be the incident directions and let $k > 0$ be the wave number. Assume that h^{app} is an approximation function of h. For $d = d_l$ consider the following linearized equations for (5.1):

$$\left(F_{d_l,k}[h^{app}]\right)(\hat{x}) + \left(F'_{d_l,k}[h^{app}; \triangle h]\right)(\hat{x}) = u^\infty_k(\hat{x}; d_l), \quad l = 1, 2, \ldots, n_d, \tag{5.2}$$

where $\triangle h$ is the update function to be determined. The Newton-type method consists in iterating (5.2) by using the Levenberg–Marquardt algorithm (see, e.g., [38]).

In the numerical experiments, we use the noisy far-field pattern $u^\infty_{\delta,k}(\hat{x}_j; d_l),\ j = 1, 2, \ldots, n_f,\ l = 1, 2, \ldots, n_d$, as the measurement data satisfying that

$$\left\| u^\infty_{\delta,k}(\cdot; d_l) - u^\infty_k(\cdot; d_l) \right\|_{L^2(\mathbb{S}^1_+)} \le \delta \left\| u^\infty_k(\cdot; d_l) \right\|_{L^2(\mathbb{S}^1_+)}, \quad l = 1, 2, \ldots, n_d,$$

where $\delta > 0$ is the noise ratio and the observation directions $\hat{x}_j,\ j = 1, 2, \ldots, n_f$, are the equidistant points on $\mathbb{S}^1_+$. In practical computation, h^{app} has to be taken from a finite-dimensional subspace R_M, where $R_M = \mathrm{span}\{\phi_{1,M}, \phi_{2,M}, \ldots, \phi_{M,M}\}$ is

a subspace of $C^2_{0,R}(\mathbb{R})$ with $\phi_{j,M},\ j = 1, 2, \ldots, M$, the spline basis functions supported in $(-R, R)$ (see Remark 5.2). Then, by the strategy in [38] we seek an update function $\triangle h = \sum_{i=1}^{M} \triangle a_i \phi_{i,M}$ in R_M which solves the minimization problem

$$\min_{\triangle a_i} \left\{ \sum_{l=1}^{n_d} \sum_{j=1}^{n_f} \left| \big(F_{d_l,k}[h^{app}]\big)(\hat{x}_j) + \big(F'_{d_l,k}[h^{app}; \triangle h]\big)(\hat{x}_j) - u^{\infty}_{\delta,k}(\hat{x}_j; d_l) \right|^2 + \beta \sum_{i=1}^{M} |\triangle a_i|^2 \right\}, \tag{5.3}$$

where $\beta > 0$ is chosen such that

$$\sum_{l=1}^{n_d} \sum_{j=1}^{n_f} \left| \big(F_{d_l,k}[h^{app}]\big)(\hat{x}_j) + \big(F'_{d_l,k}[h^{app}; \triangle h]\big)(\hat{x}_j) - u^{\infty}_{\delta,k}(\hat{x}_j; d_l) \right|^2 = \rho^2 \sum_{l=1}^{n_d} \sum_{j=1}^{n_f} \left| \big(F_{d_l,k}[h^{app}]\big)(\hat{x}_j) - u^{\infty}_{\delta,k}(\hat{x}_j; d_l) \right|^2 \tag{5.4}$$

for a given constant $\rho \in (0, 1)$. In computation, β is determined by using the bisection algorithm (see [38]). Note that β is unique if a certain assumption is satisfied (see [33]). Then the approximation function h^{app} is updated by $h^{app} + \triangle h$. Further, define the error function

$$Err_k := \frac{1}{n_d} \sum_{l=1}^{n_d} \left[\sum_{j=1}^{n_f} \left| \left(F_{d_l,k}[h^{app}]\right)(\hat{x}_j) - u^{\infty}_{\delta,k}(\hat{x}_j; d_l) \right|^2 \right]^{\frac{1}{2}} \left[\sum_{j=1}^{n_f} \left| u^{\infty}_{\delta,k}(\hat{x}_j; d_l) \right|^2 \right]^{-1/2}.$$

Then the iteration is stopped if $Err_k < \tau\delta$, where $\tau > 1$ is a fixed constant.

Remark 5.2. For a positive integer $M \in \mathbb{N}^+$ let $h = 2R/(M+5)$ and $t_i = (i+2)h - R$. Then the spline basis functions of R_M can be defined as $\phi_{i,M}(t) = \phi((t - t_i)/h), i = 1, 2, \ldots, M$, where

$$\phi(t) := \sum_{j=0}^{k+1} \frac{(-1)^j}{k!} \binom{k+1}{j} \left(t + \frac{k+1}{2} - j \right)_+^k$$

with $z_+^k = z^k$ for $z \geq 0$ and $= 0$ for $z < 0$. In this paper, we choose $k = 4$, that is, ϕ is the quantic spline function. Note that $\phi_{i,M} \in C^3(\mathbb{R})$ with support in $(-R, R)$. See [25] for details.

Remark 5.3. In the numerical experiments, the solution of the scattering problem will be computed numerically as follows.

(1) The synthetic far-field data of the scattering problem is generated by using the RCIP method introduced in section 3.1 to solve the boundary integral equations (2.14) and (2.33), in which we choose the parameter $\rho = 1$.

(2) In each iteration, we use the boundary integral method proposed in Remark 2.9 to get the numerical solution of the scattering problem to avoid the inverse crime and to reduce the complexity of the computation. Precisely, assume that $u(x; d) = u^i(x; d) + u^r(x; d) + u^s(x; d), d \in \mathbb{S}^1_-$, where u^s is the solution of the problem (NP) with the boundary Γ replaced by $\Gamma^{app} := \{(x_1, x_2) \mid x_2 = h^{app}(x_1), x_1 \in \mathbb{R}\}$. Then

the scattered field u^s is defined to be of the form (2.34), where the density function $\Phi = (\varphi_1, \varphi_2)^T$ is the solution to the integral equation (2.35). Here, the boundary Γ appearing in (2.34) and (2.35) is also replaced by Γ^{app}. Similarly as in section 3.1, the integral equation (2.35) can be numerically solved to get the approximated values of Φ on the coarse mesh. Accordingly, the far-field pattern u^∞ of the scattered field u^s can be computed with the formula (2.36) (with Γ also replaced by Γ^{app}). Further, according to Theorem 5.1 and the RCIP method introduced in section 3.1, in order to compute the Fréchet derivative at each iteration we need to compute $(d/ds)[(\nu_2 \triangle h)(du/ds)] + k^2(\nu_2 \triangle h)u$ with $\triangle h \in R_M$ at the Gauss points of each panel for the coarse mesh of $\Gamma_R^{app} := \Gamma^{app} \cap B_R$. This can be done as follows. From the formula (2.34) and the jump relation of the single-layer potential, the scattered field u^s on Γ_R^{app} is of the form

$$u^s(x) = \left(S_{k,\Gamma_R^{app} \to \Gamma_R^{app}} \varphi_1\right)(x) + \left(S_{k,\partial B_R^- \to \Gamma_R^{app}} \varphi_2\right)(x), \quad x \in \Gamma_R^{app}. \tag{5.5}$$

Then the approximated values $\mathbf{u}^{\mathrm{s}}_{\mathrm{coa}}$ of the scattered field u^s at the Gauss points for the coarse mesh of Γ_R^{app} are computed as

$$\mathbf{u}^{\mathrm{s}}_{\mathrm{coa}} = \mathbf{Q}\mathbf{L}_{\mathrm{fin}}\mathbf{\Phi}_{\mathrm{fin}}, \tag{5.6}$$

where $\mathbf{Q}$ is a restriction operator which performs panelwise 15-degree polynomial interpolation in parameter from a grid on the fine mesh to a grid on the coarse mesh, $\mathbf{L}_{\mathrm{fin}}\mathbf{\Phi}_{\mathrm{fin}}$ is the discretization of the formula (5.5) on the fine mesh, and $\mathbf{\Phi}_{\mathrm{fin}}$ is the approximated values of $\mathbf{\Phi}$ on the fine mesh which can be obtained by using a post-processor proposed in [34, section 7]. Note that the approximated values $\mathbf{u}^{\mathrm{s}}_{\mathrm{coa}}$ in (5.6) can also be obtained by using the method in [34, section 5]. In this manner, the approximated values of the total field u at the Gauss points for the coarse mesh of Γ_R^{app} are thus obtained from (5.6). Moreover, on each panel for the coarse mesh of Γ_R^{app}, we use the 15-degree polynomial interpolation to approximate the total field u on Γ_R^{app}. Finally, the first and second derivatives of the interpolation polynomial can be computed to obtain the approximated values of $(d/ds)[(\nu_2 \triangle h)(du/ds)] + k^2(\nu_2 \triangle h)u$ on Γ_R^{app}.

Now we are ready to propose the Newton-type iteration algorithm for the inverse problem. Motivated by [6], we use multifrequency far-field data in order to get an accurate reconstruction of the surface profile h. Generally speaking, the lower frequency data are used to get the main profile of the boundary, whereas the higher frequency data can be applied to get a refined reconstruction. The step of the algorithm is given as follows.

ALGORITHM 5.1. *Assume the far-field data* $u^\infty_{\delta,k_m}(\hat{x}_j; d_l), j = 1, 2, \ldots, n_f, l = 1, 2, \ldots, n_d$, $m = 1, 2, \ldots, N$, *with* $\hat{x}_j \in \mathbb{S}^1_+$, $d_l \in \mathbb{S}^1_-$, *and* $k_1 < k_2 < \cdots < k_N$.

1. *Let* $h^{app} = 0$ *be the initial guess of* h. *Set* $i = 0$ *and go to step* 2.
2. *Set* $i = i + 1$. *If* $i > N$, *then stop the iteration; otherwise, set* $k = k_i$ *and go to step* 3.
3. *If* $Err_k < \tau\delta$, *go to step* 2*; otherwise, go to step* 4.
4. *Solve* (5.3) *with the strategy* (5.4) *to get an updated function* $\triangle h$. *Let* h^{app} *be updated by* $h^{app} + \triangle h$ *and go to step* 3.

Remark 5.4. In [6], a continuation approach was proposed to reconstruct the sound-soft, locally rough surface from multifrequency scattered-field data. It was pointed out in [6] that the lowest wave number k_1 must be small enough to ensure

the main features of the surface profile to be recovered and the increment parameter $k_{j+1} - k_j$ cannot be very large since otherwise the proposed algorithm may fail to capture the Fourier modes of the exact profile between k_j and k_{j+1}. Ideally, the smaller the increment $k_{j+1} - k_j$, the better the reconstruction result. In fact, the increment $k_{j+1} - k_j$ depends on the scale feature of the real profile. Our algorithm also follows this idea to choose the multiple wave numbers (see section 5.2). For more detailed discussions on the choice of multiple wave numbers, see Remarks 5.1 and 5.2 in [6].

5.2. Numerical examples of the inverse problem. In this section, several numerical experiments are carried out to demonstrate the effectiveness of the inversion algorithm. We begin with the following assumptions in all numerical experiments.

(1) In each example, following the idea in Remark 5.4, we use multifrequency data with the wave numbers $k = 1, 2, 3, \ldots, N$, where N is the total number of frequencies. Further, we choose $N \leq 36$ and the auxiliary curve $\widetilde{\Gamma}$ is taken to be a circle with radius $r = 0.1$. It is easily checked that kr with $k = 1, 2, \ldots, 36$, are not the zeros of the Bessel function J_n for any integers n. Then, by Remark 2.5 it is valid to use the integral equation (2.14) to solve the Neumann problem (NP) for all examples.
(2) To generate the synthetic data and to compute the Fréchet derivative in each iteration, for the coarse mesh, we choose the number of panels on each smooth component n_{pan} to be the nearest integer of $0.6 * k + 18$ for each wave number k. And for the fine mesh, we choose the number of subdivisions to be $n_{sub} = 30$.
(3) We measure the half-aperture (that is, the measurement angle is between 0 and π) far-field pattern with the equidistant points $\hat{x}_j$, $j = 1, 2, \ldots, 200$. For the incident direction $d \in \mathbb{S}^1_-$, the noisy data $u^\infty_{\delta,k}(\hat{x}_j; d)$ $(j = 1, 2, \ldots, 200)$ are obtained as $u^\infty_{\delta,k}(\hat{x}_j; d) = u^\infty_k(\hat{x}_j; d) + \delta\zeta_j(\sum_{i=1}^{200} |u^\infty_k(\hat{x}_i; d)|^2)^{1/2}/(\sum_{i=1}^{200} |\zeta_i|^2)^{1/2}$, where ζ_j is a random number with $\mathrm{Re}(\zeta_j), \mathrm{Im}(\zeta_j)$ belonging to the standard normal distribution $N(0, 1)$. For all cases, we choose the noise ratio $\delta = 5\%$.
(4) We set the parameters $\rho = 0.8$ and $\tau = 1.5$.
(5) In each figure, we use a solid line "-" and a dashed line "- -" to represent the actual curve and the reconstructed curve, respectively.
(6) In all examples, for the shape of the local perturbation of the infinite plane we assume that $\mathrm{supp}(h) \in (-1, 1)$; we further choose $R = 1$ and use the smooth curves which are not in R_M.

Example 1. We first consider the surface profile $h(x_1) = \phi((x_1 + 0.2)/0.3) - 0.8\phi((x_1 - 0.3)/0.2)$, where ϕ is defined in Remark 5.2. We use the measured far-field data for two incident fields $u^i(x; d_l), l = 1, 2$, with $d_1 = (\cos(-\pi/3), \sin(-\pi/3))$ and $d_2 = (\cos(-2\pi/3), \sin(-2\pi/3))$. The auxiliary curve $\widetilde{\Gamma}$ is chosen to be the circle centered at $[-0.3, -0.4]$ and of radius $r = 0.1$. For the inverse problem, we choose the number of the spline basis functions to be $M = 40$ and the total number of frequencies to be $N = 13$. Figure 5.1 shows the reconstructed curves at $k = 1, 5, 9, 13$, respectively.

Example 2. We now consider the surface profile defined by

$$h(x_1) = \begin{cases} 0.5 \exp\left[16/(25x_1^2 - 16)\right] \cos(4\pi x_1), & |x_1| < 4/5, \\ 0, & |x_1| \geq 4/5. \end{cases}$$

We use the measured far-field data for two incident fields $u^i(x; d_l), l = 1, 2$, with $d_1 = (\cos(-\pi/3), \sin(-\pi/3))$ and $d_2 = (\cos(-2\pi/3), \sin(-2\pi/3))$. The auxiliary curve

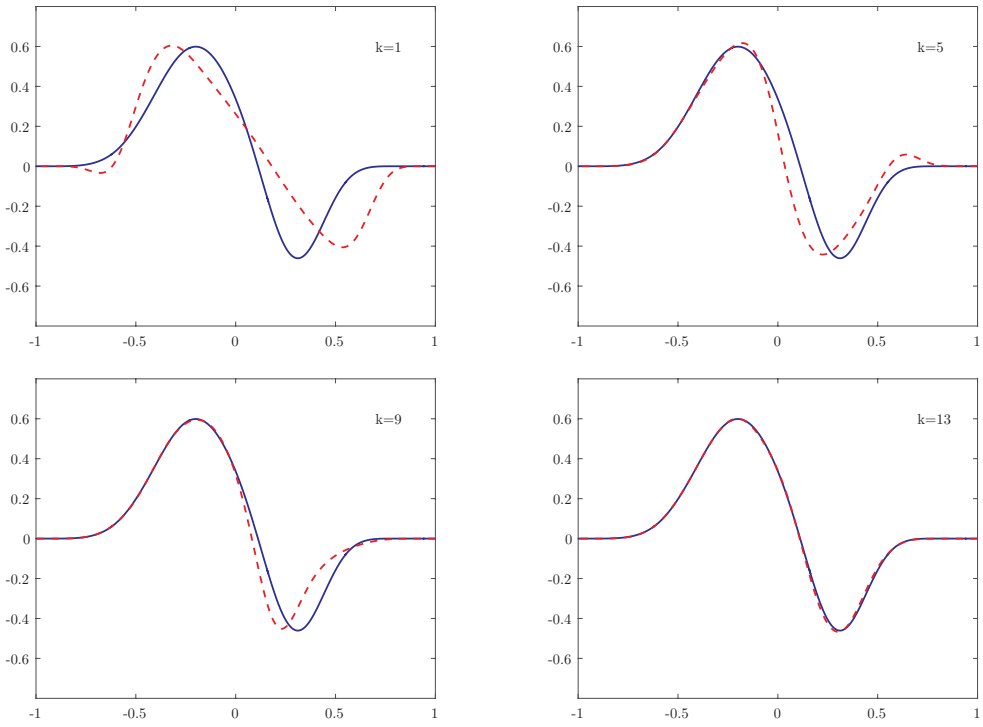

FIG. 5.1. *The reconstructed curve (dashed line) at* $k = 1, 5, 9, 13$, *respectively, from* 5% *noisy far-field data for two incident fields* $u^i(x; d_l), l = 1, 2$, *with* $d_1 = (\cos(-\pi/3), \sin(-\pi/3))$ *and* $d_2 = (\cos(-2\pi/3), \sin(-2\pi/3))$, *where the real curve is denoted by the solid line.*

$\widetilde{\Gamma}$ is chosen to be the circle centered at $[0, -0.6]$ and with radius $r = 0.1$. For the inverse problem, the number of the spline basis functions is taken to be $M = 40$ and the total number of frequencies is taken to be $N = 33$. Figure 5.2 shows the reconstructed curves at $k = 1, 11, 22, 33$, respectively.

Example 3 (multiscale profile). In this example, we consider a multiscale profile given by

$$h(x_1) = \begin{cases} \exp\left[16/\left(25x_1^2 - 16\right)\right] [0.5 + 0.1\sin(16\pi x_1)] \sin(\pi x_1), & |x_1| < 4/5, \\ 0, & |x_1| \geq 4/5. \end{cases}$$

This function is made up of two scales, that is, the macroscale part $0.5\exp[16/(25x_1^2 - 16)]\sin(\pi x_1)$ and the microscale part $0.1\exp\left[16/(25x_1^2 - 16)\right]\sin(16\pi x_1)\sin(\pi x_1)$. We use the measured far-field data for two incident fields $u^i(x; d_l), l = 1, 2$, with $d_1 = (\cos(-\pi/3), \sin(-\pi/3))$ and $d_2 = (\cos(-2\pi/3), \sin(-2\pi/3))$. We choose the auxiliary curve $\widetilde{\Gamma}$ to be the circle with center at $[0, -0.4]$ and radius $r = 0.1$. For the inverse problem, the number of the spline basis functions is chosen to be $M = 40$. To capture the two-scale features of the profile, we choose the total number of frequencies to be $N = 36$. Figure 5.3 presents the reconstructed curves at $k = 6, 18, 24, 36$, respectively. It is seen that the macroscale feature is captured at the lower frequency $k = 6$ (Figure 5.3, top left) and the microscale feature is finally captured at the highest frequency $k = 36$ (Figure 5.3, bottom right).

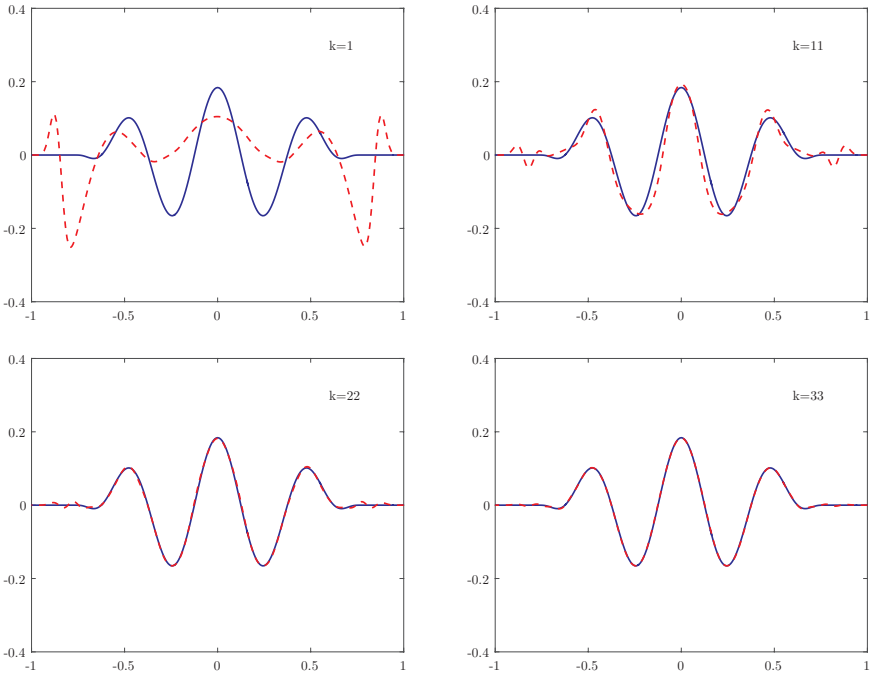

FIG. 5.2. *The reconstructed curve (dashed line) at* $k = 1, 11, 22, 33$, *respectively, from* 5% *noisy far-field data for two incident fields* $u^i(x; d_l), l = 1, 2$, *with* $d_1 = (\cos(-\pi/3), \sin(-\pi/3))$ *and* $d_2 = (\cos(-2\pi/3), \sin(-2\pi/3))$, *where the real curve is denoted by the solid line.*

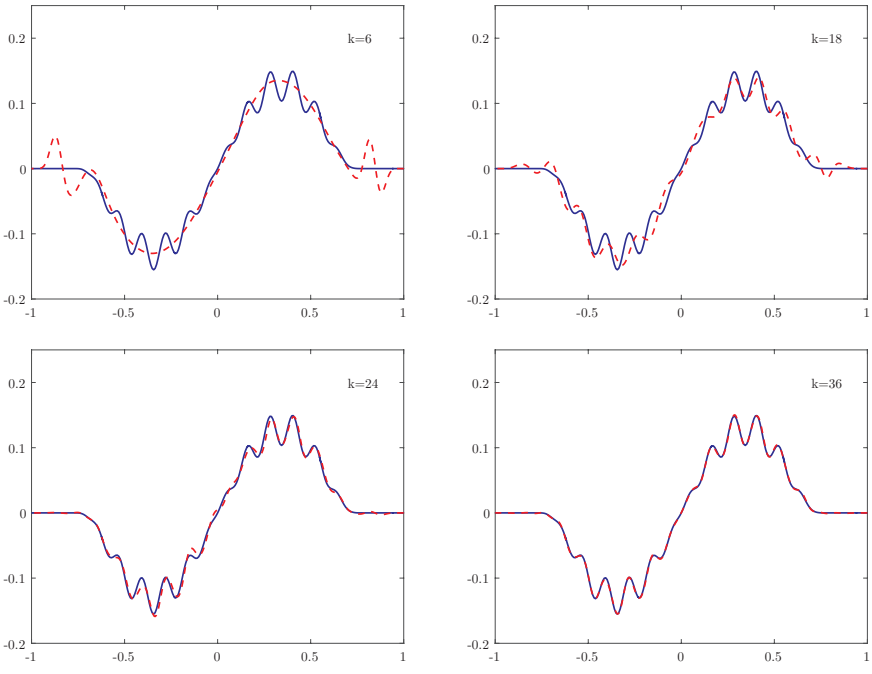

FIG. 5.3. *The reconstructed curve (dashed line) at* $k = 6, 18, 24, 36$, *respectively, from* 5% *noisy far-field data for two incident fields* $u^i(x; d_l), l = 1, 2$, *with* $d_1 = (\cos(-\pi/3), \sin(-\pi/3))$ *and* $d_2 = (\cos(-2\pi/3), \sin(-2\pi/3))$, *where the real curve is represented by the solid line.*

6. Conclusion. We considered the scattering problem by a locally rough surface on which the Neumann boundary condition is imposed. An equivalent novel integral equation formulation was proposed for the direct scattering problem, and a fast and efficient numerical algorithm was further given to solve the integral equation, based on the RCIP method previously introduced by Helsing. The far-field pattern of the scattering problem can then be computed accurately by using the fast and efficient integral equation solver. For the inverse problem, we proved that the locally rough surface is uniquely determined from a knowledge of the far-field pattern associated with incident plane waves. Further, a Newton-type iteration algorithm with multi-frequency far-field data is also developed to reconstruct the locally rough surface, where the proposed novel integral equation is applied to solve the direct scattering problem in each iteration. Numerical experiments demonstrate that our inversion algorithm is stable and accurate even for the case of multiple scale surface profiles. It is interesting to extend our method to the three-dimensional Helmholtz and Maxwell equations which are more challenging.

Acknowledgments. We thank Professor Johan Helsing for useful discussions on the RCIP method and especially for his open MATLAB codes, which are very helpful. We thank the referees for their constructive comments, which helped to improve the presentation of this paper.

REFERENCES

[1] H. Ammari, G. Bao, and A. W. Wood, *An integral equation method for the electromagnetic scattering from cavities*, Math. Methods Appl. Sci., 23 (2000), pp. 1057–1072.
[2] G. Bao, J. Gao, and P. Li, *Analysis of direct and inverse cavity scattering problems*, Numer. Math. Theory Methods Appl., 4 (2011), pp. 419–442.
[3] G. Bao, G. Hu, and T. Yin, *Time-harmonic acoustic scattering from locally perturbed half-planes*, SIAM J. Appl. Math., 78 (2018), pp. 2672–2691.
[4] G. Bao and P. Li, *Near-field imaging of infinite rough surfaces*, SIAM J. Appl. Math., 73 (2013), pp. 2162–2187.
[5] G. Bao and P. Li, *Near-field imaging of infinite rough surfaces in dielectric media*, SIAM J. Imaging Sci., 7 (2014), pp. 867–899.
[6] G. Bao and J. Lin, *Imaging of local surface displacement on an infinite ground plane: The multiple frequency case*, SIAM J. Appl. Math., 71 (2011), pp. 1733–1752.
[7] G. Bao and L. Zhang, *Shape reconstruction of the multi-scale rough surface from multifrequency phaseless data*, Inverse Problems, 32 (2016), 085002.
[8] J. Bremer, *A fast direct solver for the integral equations of scattering theory on planar curves with corners*, J. Comput. Phys., 231 (2012), pp. 1879–1899.
[9] O. P. Bruno, J. S. Ovall, and C. Turc, *A high-order integral algorithm for highly singular PDE solutions in Lipschitz domains*, Computing, 84 (2009), pp. 149–181.
[10] C. Burkard and R. Potthast, *A multi-section approach for rough surface reconstruction via the Kirsch–Kress scheme*, Inverse Problems, 26 (2010), 045007.
[11] C. Burkard and R. Potthast, *A time-domain probe method for three-dimensional rough surface reconstructions*, Inverse Problems Imaging, 3 (2009), pp. 259–274.
[12] G. A. Chandler, *Galerkin's method for boundary integral equations on polygonal domains*, J. Aust. Math. Soc. B, 26 (1984), pp. 1–13.
[13] S. N. Chandler-Widle and A. T. Peplow, *A boundary integral equation formulation for the Helmholtz equation in a locally perturbed half-plane*, Z. Angew. Math. Mech., 85 (2005), pp. 79–88.
[14] S. N. Chandler-Widle and B. Zhang, *A uniqueness result for scattering by infinite rough surfaces*, SIAM J. Appl. Math., 58 (1998), pp. 1774–1790.
[15] S. N. Chandler-Wilde, C. R. Ross, and B. Zhang, *Scattering by infinite one-dimensional rough surfaces*, Proc. A, 455 (1999), pp. 3767–3787.
[16] S. N. Chandler-Widle and B. Zhang, *Scattering of electromagnetic waves by rough interfaces and inhomogeneous layers*, SIAM J. Math. Anal., 30 (1999), pp. 559–583.

[17] S. N. Chandler-Wilde and P. Monk, *Existence, uniqueness and variational methods for scattering by unbounded rough surfaces*, SIAM J. Math. Anal., 37 (2005), pp. 598–618.
[18] S. N. Chandler-Wilde, E. Heinemeyer, and R. Potthast, *A well-posed integral equation formulation for three-dimensional rough surface scattering*, Proc. A, 462 (2006), pp. 3683–3705.
[19] S. N. Chandler-Wilde, E. Heinemeyer, and R. Potthast, *Acoustic scattering by mildly rough unbounded surfaces in three dimensions*, SIAM J. Appl. Math., 66 (2006), pp. 1002–1026.
[20] S. N. Chandler-Wilde and J. Elschner, *Variational approach in weighted Sobolev spaces to scattering by unbounded rough surfaces*, SIAM J. Math. Anal., 42 (2010), pp. 2554–2580.
[21] S. N. Chandler-Wilde and C. Lines, *A time domain point source method for inverse scattering by rough surfaces*, Computing, 75 (2005), pp. 157–180.
[22] Y. Chen, O. R. Spivack, and M. Spivack, *Rough surface reconstruction from phaseless single frequency data at grazing angles*, Inverse Problems, 34 (2018), 124002.
[23] R. Coifman, M. Goldberg, T. Hrycak, M. Israeli, and V. Rokhlin, *An improved operator expansion algorithm for direct and inverse scattering computations*, Waves Random Media, 9 (1999), pp. 441–457.
[24] D. Colton and R. Kress, *Inverse Acoustic and Electromagnetic Scattering Theory*, 3rd ed., Springer, New York, 2013.
[25] C. de Boor, *A Practical Guide to Splines*, Springer, New York, 2001.
[26] M. Durán, I. Muga, and J. C. Nédélec, *The Helmholtz equation in a locally perturbed half-plane with passive boundary*, IMA J. Appl. Math., 71 (2006), pp. 853-876.
[27] M. Durán, I. Muga, and J. C. Nédélec, *The Helmholtz equation in a locally perturbed half-space with non-absorbing boundary*, Arch. Ration. Mech. Anal., 191 (2009), pp. 143–172.
[28] J. A. DeSanto and R. J. Wombell, *Reconstruction of rough surface profiles with the Kirchhoff approximation*, J. Opt. Soc. Amer. A, 8 (1991), pp. 1892–1897.
[29] J. A. DeSanto and R. J. Wombell, *The reconstruction of shallow rough-surface profiles from scattered field data*, Inverse Problems, 7 (1991), pp. L7–L12.
[30] M. Ding, J. Li, K. Liu, and J. Yang, *Imaging of local rough surfaces by the linear sampling method with near-field data*, SIAM J. Imaging Sci., 10 (2017), pp. 1579–1602.
[31] W. Lu, Y. Lu, and J. Qian, *Perfectly matched layer boundary integral equation method for wave scattering in a layered medium*, SIAM J. Appl. Math., 78 (2018), pp. 246–265.
[32] L. Feng and F. Ma, *Uniqueness and local stability for the inverse scattering problem of determining the cavity*, Sci. China A Math., 48 (2005), pp. 1113–1123.
[33] M. Hanke, *A regularizing Levenberg-Marquardt scheme, with applications to inverse groundwater filtration problems*, Inverse Problems, 13 (1997), pp. 79–95.
[34] J. Helsing, *Integral equation methods for elliptic problems with boundary conditions of mixed type*, J. Comput. Phys., 228 (2009), pp. 8892–8907.
[35] J. Helsing, *Solving Integral Equations on Piecewise Smooth Boundaries Using the RCIP Method: A Tutorial*, arXiv:1207.6737v9, 2018.
[36] J. Helsing and A. Karlsson, *An accurate boundary value problem solver applied to scattering from cylinders with corners*, IEEE Trans. Antennas Propagation, 61 (2013), pp. 3693–3700.
[37] J. Helsing and S. Jiang, *On integral equation methods for the first Dirichlet problem of the biharmonic and modified biharmonic equations in nonsmooth domains*, SIAM J. Sci. Comput., 40 (2018), pp. A2609–A2630.
[38] T. Hohage, *Iterative Methods in Inverse Obstacle Scattering: Regularization Theory of Linear and Nonlinear Exponentially Ill-Posed Problems*, Ph.D. thesis, University of Linz, Austria, 1999.
[39] R. Kress and T. Tran, *Inverse scattering for a locally perturbed half-plane*, Inverse Problems, 16 (2000), pp. 1541–1559.
[40] P. Li, *An inverse cavity problem for Maxwell's equations*, J. Differential Equations, 252 (2012), pp. 3209–3225.
[41] J. Li and G. Sun, *A nonlinear integral equation method for the inverse scattering problem by sound-soft rough surfaces*, Inverse Probl. Sci. Eng., 23 (2015), pp. 557–577.
[42] J. Li, G. Sun, and B. Zhang, *The Kirsch-Kress method for inverse scattering by infinite locally rough interfaces*, Appl. Anal., 96 (2017), pp. 85–107.
[43] X. Liu, B. Zhang, and H. Zhang, *A direct imaging method for inverse scattering by unbounded rough surfaces*, SIAM J. Imaging Sci., 11 (2018), pp. 1629–1650.
[44] W. McLean, *Strongly Elliptic Systems and Boundary Integral Equations*, Cambridge University Press, Cambridge, UK, 2000.
[45] M. Spivack, *Direct solution of the inverse problem for rough scattering at grazing incidence*, J. Phys. A, 25 (1992), pp. 3295–3302.

[46] A. Willers, *The Helmholtz equation in disturbed half-spaces*, Math. Methods Appl. Sci., 9 (1987), pp. 312–323.
[47] A. Wood, *Analysis of electromagnetic scattering from an overfilled cavity in the ground plane*, J. Comput. Phys., 215 (2006), pp. 630–641.
[48] B. Zhang and S. N. Chandler-Wilde, *Integral equation methods for scattering by infinite rough surfaces*, Math. Methods Appl. Sci., 26 (2003), pp. 463–488.
[49] B. Zhang and H. Zhang, *Imaging of locally rough surfaces from intensity-only far-field or near-field data*, Inverse Problems, 33 (2017), 055001.
[50] H. Zhang and B. Zhang, *A novel integral equation for scattering by locally rough surfaces and application to the inverse problem*, SIAM J. Appl. Math., 73 (2013), pp. 1811–1829.